Quaternary Science Reviews 149 (2016) 288–305

Contents lists available at ScienceDirect

Quaternary Science Reviews

journal homepage: www.elsevier.com/locate/quascirev

Complex patterns of glacier advances during the late glacial in the Chagan Uzun Valley, Russian Altai

Natacha Gribenski [a, b, *], Krister N. Jansson [a, b], Sven Lukas [c], Arjen P. Stroeven [a, b], Jonathan M. Harbor [a, b, d], Robin Blomdin [a, b], Mikhail N. Ivanov [e], Jakob Heyman [f], Dmitry A. Petrakov [e], Alexei Rudoy [g], Tom Clifton [h], Nathaniel A. Lifton [d, h], Marc W. Caffee [d, h]

[a] Geomorphology & Glaciology, Department of Physical Geography, Stockholm University, Sweden
[b] Bolin Centre for Climate Research, Stockholm University, Sweden
[c] School of Geography, Queen Mary University of London, UK
[d] Department of Earth, Atmospheric, and Planetary Sciences, Purdue University, USA
[e] Faculty of Geography, Lomonosov Moscow State University, Russia
[f] Department of Earth Sciences, University of Gothenburg, Sweden
[g] Department Geology and Geography, National Research Tomsk State University, Russia
[h] Department of Physics and Astronomy, Purdue Rare Isotope Measurement Laboratory (PRIME Lab), Purdue University, USA

ARTICLE INFO

Article history:
Received 7 March 2016
Received in revised form
25 July 2016
Accepted 26 July 2016
Available online 11 August 2016

Keywords:
Altai
Paleoglaciation
Surging glacier
Geomorphology
Sedimentology
^{10}Be and ^{26}Al surface exposure dating
Moraines

ABSTRACT

The Southern part of the Russian Altai Mountains is recognized for its evidence of catastrophic glacial lake outbursts. However, little is known about the late Pleistocene paleoglacial history, despite the interest in such reconstructions for constraining paleoclimate. In this study, we present a detailed paleoglaciological reconstruction of the Chagan Uzun Valley, in the Russian Altai Mountains, combining for the first time detailed geomorphological mapping, sedimentological logging, and *in situ* cosmogenic ^{10}Be and ^{26}Al surface exposure dating of glacially-transported boulders. The Chagan Uzun Valley exhibits the most impressive glacial landforms of this sector of the Altai, with extensive lobate moraine belts deposited in the intramontane Chuja Basin, reflecting a series of pronounced former glacial advances. Observations of "hillside-scale" folding and extensive faulting of pre-existing soft sediments within the outer moraine belts, together with the geomorphology, strongly indicate that these moraine belts were formed during surge-like events. Identification of surge-related features is essential for paleoclimate inference because these features correspond to a glacier system that is not in equilibrium with the contemporary climate, but instead largely influenced by various internal and external factors. Therefore, no strict relationship can be established between climatic variables and the pronounced distal glacial extent observed in the Chagan Uzun Valley/Chuja basin. In contrast, the inner (up-valley) glacial landforms of the Chagan Uzun valley were likely deposited during retreat of temperate valley glaciers, close to equilibrium with climate, and so most probably triggered by a general warming. Cosmogenic ages associated with the outermost, innermost, and intermediate moraines all indicate deposition times clustered around 19 ka. However, the actual deposition time of the outermost moraine may slightly predate the ^{10}Be ages due to shielding caused by subsequent lake water coverage. This chronology indicates a Marine Isotope Stage (MIS) 2 last maximum extent of the Chagan Uzun Glacier, and an onset of the deglaciation around 19 ka. This is consistent with other regional paleoclimate proxy records and with the Northern Hemisphere glaciation chronology. Finally, this study also highlights the highly dynamic environment in this area, with complex interactions between glacial events and the formation and drainage of lakes.

* Corresponding author. Geomorphology & Glaciology, Department of Physical Geography, Stockholm University, Sweden.
E-mail address: natacha.gribenski@natgeo.su.se (N. Gribenski).

http://dx.doi.org/10.1016/j.quascirev.2016.07.032
0277-3791/

1. Introduction

Reconstructions of the former extents of mountain glaciers can be a useful paleoclimate proxy because their advance and retreat are largely controlled by changes in temperature and precipitation (Cuffey and Paterson, 2010). However, non-climatic factors (such as internal ice dynamics, topography or bed geology) can also influence the advance or retreat of a glacier (e.g., Benn and Lehmkuhl, 2000; Glasser et al., 2005). Moreover, the fragmented nature of preserved glacial landforms and difficulties in constraining their ages are additional uncertainties to be considered when using such records for paleoclimate reconstructions (Kirkbride and Brazier, 1998; Kirkbride and Winkler, 2012; Barr and Lovell, 2014). Despite these limitations this archive offers considerable advantage relative to more traditional high-resolution stratigraphic and continuous proxies (e.g., ice-core, lacustrine, and speleothem records): their wide geographical distribution provides a broader distribution of location-specific nodes yielding information about former local or regional climate conditions (Schaefer et al., 2006; Kirkbride and Winkler, 2012). This information is particularly useful for testing and developing general circulation models (GCM) (Solomina et al., 2008; Jomelli et al., 2009), especially for areas located at the confluence of major climatic systems because these regions are more sensitive to changes in atmospheric circulation patterns (Rupper and Roe, 2008).

Central Asia, which comprises the Pamir, Tian Shan, Kunlun, and Altai mountains (Fig. 1), is located at the confluence of mid-latitude Westerlies and the Siberian High pressure system (Aizen et al., 2006; Shahgedanova et al., 2010). Numerous mountain glaciers and associated landforms have been mapped in this region (eg., Sapozhnikov, 1911; Novikov, 1988; Butvilovsky, 1993; Bussemer, 2001; Shahgedanova et al., 2010; Stroeven et al., 2013; Blomdin et al., 2016). Despite the potential of the area for understanding the climate system, relatively few studies provide robust paleoglacial reconstructions, especially within the Altai Mountains.

This paper provides a detailed paleoglacial reconstruction of the Chagan Uzun valley, located in the Kuray-Chuja intermontane basin area, in the southeastern part of the Russian Altai (Fig. 1). This area has attracted attention due to its history of extensive glacier-impounded paleolakes and related discharge events (e.g. Rudoy, 1981, 2002; Rudoy and Baker, 1993; Carling et al., 2002; Herget, 2005; Reuther et al., 2006), reported as among the largest flood events on Earth (Baker et al., 1993; Margold et al., 2011). Reconstructions of these ice-dammed lakes and their dynamics have also been used to infer the timing of former glacier expansions and retreat (Okishev, 1982; Rudoy and Baker, 1993; Reuther et al., 2006). The first descriptive paleoglacial studies of the Chagan Uzun valley appear in the 1960s (Shukina, 1960; Popov, 1962), while the first attempts at absolute dating were done in 1970s (Svitoch, 1978; Svitoch and Parunin, 1976). However, the ages were unreliable due to methodological weaknesses. Likewise, there is a lack of reliable age control for glacial features in the Kuray-Chuja basin area, which has thus far hampered the reconstruction of reliable glacier chronologies in this area. In this study, we focus on understanding the former glacial dynamics from the glacial deposits identified in the Chagan Uzun Valley. Detailed geomorphological and sedimentological investigations provide a framework for *in situ* cosmogenic ^{10}Be and ^{26}Al surface exposure dating and for making paleoclimate inferences. We also discuss the interaction between glacial advances and lake formation and drainage.

1.1. General geographical context

The Chagan Uzun Valley is located in the southern part of the Russian Altai Mountains, in Central Asia (Fig. 1). The Altai Mountains extend more than 1500 km across the borderlands between Kazakhstan, Russia, China and Mongolia, comprising alternating ranges and tectonic depressions that are roughly orientated NW-SE and E-W. The large-scale arrangement is controlled by sub-parallel and subsidiary intersecting fault systems, primarily originating from India-Eurasia convergence (Delvaux et al., 1995).

Key topographic features within the southern Russian Altai are the Kuray and Chuja basins: two large and interconnected basins drained by the Chuja River (Fig. 1). These tectonic depressions, initiated in the late Eocene-Oligocene, have been enhanced by intense vertical movement of around 2500 m during the late Pliocene and subsequently filled with up to 1200 m of sediments (Delvaux et al., 1995; Carling et al., 2002). The Kuray and Chuja

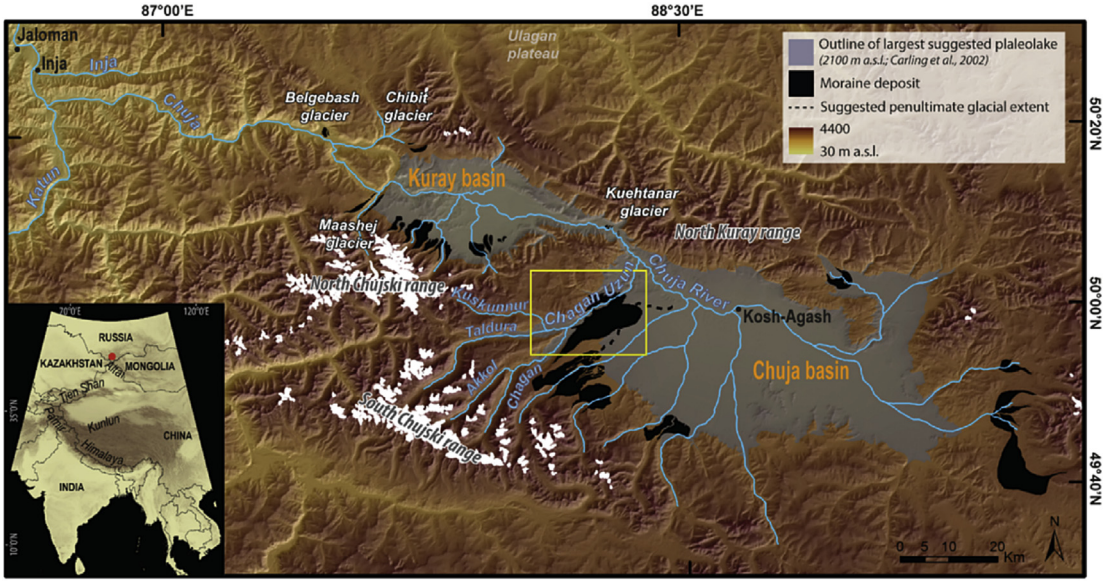

Fig. 1. The general geomorphological setting of the region. The Chagan Uzun Valley is located at the south-western margin of the Chuja basin. Yellow box and red dot in the inset map show the study area. (For interpretation of the references to colour in this figure legend, the reader is referred to the web version of this article.)

basins, with floors at ~1500 and ~1700–1800 m above sea level (m a.s.l.), respectively, are bounded by the North Kuray Range to the north, and the North and South Chujski ranges to the south. Individual peaks reach altitudes above 4000 m a.s.l. (Fig. 1). Numerous lobate moraine complexes, formed during previous periods of glacier expansion, are concentrated at the southern margin of the basins. The most prominent series of these lobate moraines occurs in the southwestern part of the Chuja basin along the Chagan Uzun valley (Fig. 1).

The Chagan and the Taldura rivers join to form the Chagan Uzun River, which cuts through the Chagan Uzun glacial deposits for more than 15 km, and then joins the Chuja River (Fig. 1). The catchment of the Chagan Uzun drainage system is predominantly composed of gneisses and schists, but also includes sedimentary and lightly metamorphosed rocks (sandstones, siltstones and sericite-chlorite shales) and granitic intrusions (Dmitrieva et al., 1959). Numerous seismic dislocation features attest to the high tectonic activity of the area (Rogozhin et al., 2007). It is likely that large-magnitude earthquakes have triggered large landslides in the area, as in 2003, when an M_S 7.5 earthquake triggered the detachment of a mass of ~3.10^7 m^3 along the Chagan-Taldura interfluve (Rogozhin et al., 2007).

1.2. Glacial lakes of the Kuray and Chuja basins

The interconnected Kuray and Chuja basins, which are enclosed by high mountain ranges (Fig. 1), form an ideal setting for the development of ice-impounded lakes. Glaciers expanding across narrow gorges at the exit of the Kuray Basin (Maaschej Glacier, emanating from the North Chujski Range, and Chibit and Belgebash glaciers emanating from the North Kuray Range) and between the Kuray and Chuja basins (Kuehtanar Glacier; Fig. 1) are considered to have repetitively dammed the Chuja River in the past (Rudoy, 1981; Baker et al., 1993; Herget, 2005). River damming by glaciers has caused the repeated formation of extensive glacial lakes within either one or both basins (Obruchev, 1914; Okishev, 1982; Baker et al., 1993; Rudoy and Baker, 1993; Rudoy, 1998). The existence of these paleo-lakes is confirmed by the presence of lacustrine sediments and numerous shorelines in the Kuray and Chuja basins, between 1615 and 2000 m a.s.l. and 1940–2100 m a.s.l., respectively (Carling et al., 2002, 2011). Higher lake levels, up to 2250 m a.s.l., have been suggested by other authors (Rudoy, 2002; Rusanov, 2008) but remain unconfirmed (Herget, 2005; Bohorquez et al., 2015). Isolated large boulders on basin floors and on shorelines have previously been interpreted as dropstones melted out from icebergs drifting on these lakes (Rudoy, 1981; Carling, 1996; Carling et al., 2011). Landslide deposits identified near the mouth of the Kuehtanar Valley (Fig. 1) have also been suggested as having temporarily dammed the Chuja River. However, this process could only generate minor lakes (maximum elevation of 1750 m a.s.l.) in the Chuja Basin alone (Butvilovsky, 1993; Agatova et al., 2014).

Sudden drainage of the largest of these late Pleistocene glacial lakes produced peak discharges that are among the largest known on Earth (>10^7 m^3 s^{-1}) (e.g., Baker et al., 1993; Rudoy, 2002; Herget, 2005; Reuther et al., 2006). Main evidence for these catastrophic drainage events are large gravel dune fields found in the two basins and further downstream in the Katun Valley (Carling, 1996; Rudoy, 1998; Carling et al., 2002) and giant gravel bars at the confluence of the Chuja and Katun rivers, near the villages of Inja and Jaloman (Rudoy and Baker, 1993; Carling et al., 2002; Herget, 2005) (Fig. 1). A sequence of three lacustrine units interbedded with flood gravel deposits has been identified in Inja Valley (Fig. 1), providing evidence for at least three flooding events (Carling et al., 2002; Herget, 2005), although it is likely that more events occurred during the Pleistocene (Rudoy, 1998, 2002; Carling et al., 2002; Herget, 2005). Based on ^{10}Be ages obtained from boulders located on the giant gravel bars near Jaloman and from dropstones in both basins, Reuther et al. (2006) dated the last and largest late Pleistocene cataclysmic flood in the area (lake level ~2100 m a.s.l. and water volume ~600 km^3) at 15.8 ± 1.8ka (original age calculated using Stone (2000) production rate and Lal (1991)/Stone (2000) scaling factor). However, recalculating these ^{10}Be ages using the recent production rate by Borchers et al. (2016) and the "Sa" scaling scheme of Lifton et al. (2014), as used in this study (cf Methods, section 2.), upgrades the timing of this outburst event to 18.7 ± 1.6 ka.

A much smaller lake, with an elevation up to 1800 m a.s.l. at its maximum filling, is suggested to have existed nearly throughout the entire Holocene (Rusanov, 2010; Agatova et al., 2014). The timing of this smaller lake is based on the presence of Late Pleistocene Holocene ostracode fauna in lacustrine sediments located around 1750–1800 m a.s.l, and on radiocarbon dates from soil formation post-dating the existence of this lake (Agatova et al., 2014). Additional chronological data associated with lake episodes and/or drainage events are reported in the literature ca. 15, 20, 25, 32 and > 45 ka. These ages are based on radiocarbon and thermoluminescence dating of lacustrine deposits, shorelines and alluvial units (Carling et al., 2002; Herget, 2005). However, the lack of documentation regarding the methods used and characteristics of the sampled material hampers an assessment of data quality.

1.3. Existing chronological constraints on the glacial history

Despite the rich record of glacial landforms identified in the Russian Altai (Popov, 1962; Butvilovsky, 1993; Blomdin et al., 2016), especially along the southern margins of the Chuja and Kuray basins, there is a lack of robust chronological data for inferring the glacial expansion and retreat patterns in this region.

Several attempts using different techniques to date the moraine deposits in the Kuray-Chuja basin area (including the Chagan Uzun valley) have been made over the past. These include radiocarbon (e.g, Markov, 1978; Okishev, 1982; Butvilovsky, 1993), varve-counting (Sheinkman, 2011), thermoluminescence (Svitoch, 1978; Rudoy, 1998; Sheinkman, 2011) and Optically-Stimulated Luminescence (Infra-red wave length stimulation, IRSL; Lehmkuhl et al., 2007). These data provide highly variable glacial chronologies, with a last glacial maximum timing varying from ~20 ka (Lehmkuhl et al., 2007) to ~60 ka (Svitoch, 1978) or >80 ka (Sheinkman, 2011), and additional glacial advances suggested between ~20 and 30 ka (Markov, 1978; Okishev, 1982; Butvilovsky, 1993; Rudoy, 1998) and ~13 ka (Okishev, 1982; Butvilovsky, 1993). However, most of these chronological data have to be considered cautiously because of the limitations of the applied methods, given the geologic setting, or because of insufficient documentation. For example, an important constraint when using OSL techniques is the need for full signal resetting (bleaching) prior to deposition of sediments. The bleaching efficiency depends on sediments daylight exposure, which has been shown to be problematic in glacial settings and might therefore lead to an overestimation of ages (e.g., Gemmell, 1988; Duller, 2006; Lukas et al., 2007; Alexanderson and Murray, 2012; Blomdin et al., 2012). Full resetting is even more challenging when using TL, because it requires longer light exposure time and a source of heat, which is also problematic in glacial environments (Forman, 1988). The varve-counting approach adopted by Sheinkman (2011) lacks a robust description of the methodology and so the reliability of the ages cannot be independently assessed. Likewise, for most of the pre-Holocene ^{14}C ages from this area, insufficient information regarding sample characteristics and/or locations hampers an evaluation of their reliability and their use.

The development of cosmogenic dating techniques in the late 20th century led to major advances in geochronology and is currently widely used in geomorphology, including paleoglaciology (Cerling and Craig, 1994; Fabel and Harbor, 1999; Cockburn and Summerfield, 2004; Balco, 2011). Reuther (2007) applied ^{10}Be surface exposure dating on moraines from the Chibit and Maschej glaciers (Fig. 1) to reconstruct the Late Pleistocene glacial history of the area. They found well-clustered exposure ages with a mean of 13.8 ± 1.4 ka for the Chibit Glacier moraine (ages calculated using Stone (2000) production rate and Lal (1991)/Stone (2000) scaling factor) but were unable to obtain reliable ages for the Maschej Glacier moraine due to low quartz contents of the collected samples. They also sampled three boulders in the Chagan Uzun valley. However, besides poor AMS performance for two of the boulders, their deposition couldn't be unequivocally related to a Chagan Uzun glacier advance and they were rather regarded as dropstones. In addition to the 13.8 ± 1.4 ka glacial extent, Reuther et al. (2006) suggested an earlier glacial advance period before 16 ka, based on the paleolake outburst dated at 15.8 ± 1.8 ka (cf section 1.2), which was attributed to the climatically-induced downwasting of the ice dam. However, updated ^{10}Be ages (using Borchers et al. (2016) production rate and Lifton et al. (2014) "Sa" scaling factor), shows that the Chibit moraine were most probably formed around 16.3 ka and the paleolake outburst occurred around 18.7 ka. Finally, evidence for Late Holocene (Little Ice Age (13th to 18th century) and 2.3 to 1.7 ka) glacial re-advances are reported by Agatova et al. (2014), based on radiocarbon dating and dendrochronology applied to several glacial valleys in the south-eastern Russian Altai.

Paleoglacial studies performed in the Chuja River basin show a lack of robust and direct glacial chronologies and highlight the need of detailed dating campaigns with suitable techniques to identify the patterns of glacier expansion and retreat in the Southern Russian Altai. This study presents a detailed geomorphological and chronological reconstruction of the paleoglacial history in the Chagan Uzun Valley, located in the South Russian Altai, relying on remote sensing analysis, field evidence and using *in situ* ^{10}Be surface exposure dating.

2. Methods

2.1. Geomorphological mapping

Detailed geomorphological mapping covering 750 km^2 was conducted in the Chagan Uzun Valley. To reconstruct former ice extent, dynamics, and flow directions, the following glacial landforms were mapped using criteria summarized in Table 1: moraine ridges, meltwater channels, and ice-scoured landscapes. In addition, major landforms and deposits of non-glacial origin, intrinsically linked with the geomorphic evolution of the area (landslides associated features and extensive lacustrine deposits), were also recorded.

Preliminary "on-screen" mapping was carried out, based on SPOT-6 (date: 10-12-2013, time 04:48 (UTC)) and Landsat 7 ETM + satellite imagery, Google Earth, and digital elevation models (ASTER and SRTM, resolution 30 m and 90 m, respectively) in ArcMap GIS software (Fig. 2). The mapping was field-checked during the summers of 2013 and 2014. The final map is displayed in the WGS1984-UTM45N coordinate system, using an elevation layer map produced from the ASTER DEM draped with transparent SRTM hill shade in greyscale as a background.

2.2. Sedimentology

The study area contained a number of natural exposures of sedimentary sections but only two are related directly to glacial landforms and, therefore, of relevance in understanding former glacier dynamics. Measured detailed two-dimensional logs on square millimetre paper were made in the field for each exposure, using markers at regular intervals along the base of the section and a tape measure hung from the top of the exposure as a vertical scale. Prominent boulders and unit boundaries were drawn first, with detail being added progressively. A photomosaic for each section was also recorded. Individual sedimentary units were identified and distinguished on the basis of their visual physical properties including grain size range, sorting, compaction, sedimentary structures (depositional, erosional and deformation structures), and clast shape, roundness, colour and lithology. The nature of contacts between individual units was also recorded. A lithofacies code is employed for effective and rapid description using the standard of Evans and Benn (2004) and Benn and Evans (2010). The orientation of key landscape features (e.g., moraine crestlines and valley axes), and the strike and dip of moraine surface slopes, planar contacts between selected prominent lacustrine units, fault planes, and fold limbs were measured using a modified Recta compass-clinometer with a liquid level following established protocols (e.g. Lukas, 2005, 2012; Lukas et al., 2012). Plotting and statistical analysis of structural data was carried out in GeOrient (Holcombe, 2010).

2.3. Ice surface profile reconstruction

Former ice surface profiles were reconstructed using the Excel spreadsheet program *Profiler v.2* distributed by Benn and Hulton (2010). The program adopts a "perfectly plastic" ice rheology, and requires the following inputs for each step (*x* co-ordinate) along the

Table 1
Identification criteria and significance of landforms and deposits mapped in the Chagan Uzun Valley.

Landform	Identification criteria	Significance
Moraine ridge	Prominent ridges extended across valley floors and/or along valley sides. Linear, curved, sinuous or saw-toothed plan form.	Former glacier margin terminal position.
Meltwater channels	Linear depression on bedrock or sediment. Can be parallel to, or cross-cut, the valley slope. Can also be parallel to, or cross-cut, moraine deposits.	Indicates former ice margin position, as meltwater following the ice margin incises the channels.
Roches moutonnées	Bare bedrock features, with stoss- and lee-side topography. Glacial lineations on rock surface.	Indication of ice flow direction. Basal ice at the pressure-melting point.
Lacustrine deposits	Thick and extensive deposit of silt sediments. Yellow-beige color in true colour images.	Former lake presence.
Landslide features	Scar: edge located on upper slope part, marking abrupt slope break, with near vertical slope below the scarp. Linear, more or less concave shape downward.Landslide deposit: Massive unconsolidated accumulation of unsorted material. Located at the base of the slope, usually overhung by scarp.	Mass movement.

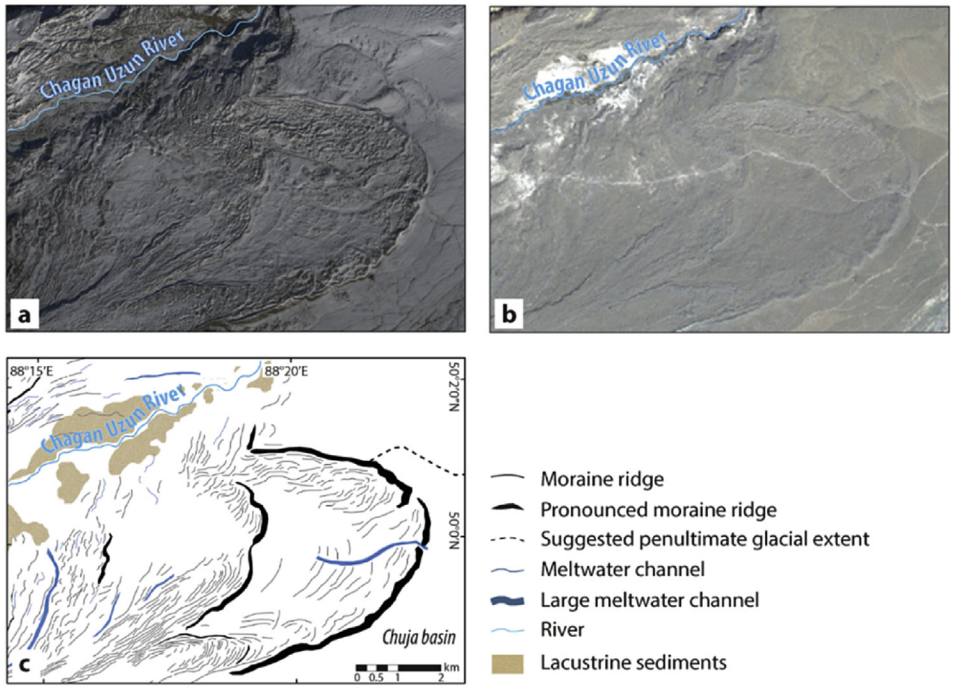

Fig. 2. Example of landforms observed in the Chagan Uzun Valley (zoom on the distal glacial landforms) displayed in (a) SPOT image and (b) Landsat 7 ETM + image and (c) associated geomorphological map.

longitudinal profile: bed elevation, a shape factor (f) accounting for valley side-drag effects, and a basal shear stress value (τ_B, kPa). These reconstructions have been performed to investigate the potential connection between lateral and frontal moraines and to identify the type of glacier system (e.g., valley glaciers sourced from cirques or nourished by an ice cap).

Bed elevations were extracted from the ASTER DEM in ArcGIS along a flowline beginning at the former glacier terminus, on the outermost margin of the Chagan Uzun lobate moraines. The flowline crosses then through all of the Chagan Uzun deposits and continues through the connected Chagan and Akkol glacial valley (Fig. 1) until reaching the top of the headwall. A grid step of 500 m (yielding a total of 112 grid points) was used. A shape factor $f = 1$ was applied along the lower profile (grid points 1 to 33) where the glacier was advancing in an open area without confining walls, and a shape factor of $f = 0.6$ was adopted in the upper section (grid points 34 to 112) where the glacier was confined to a glacial valley. These values were based on averaged shape factors calculated for several cross section geometries (from the ASTER DEM) along the valleys using the *shape factor calculator* spread sheet of Benn and Hulton (2010). Different basal shear stress values have been used, from 10 to 200 kPa, to span the range of stress values reported in the literature for different geological settings (hard or soft bedrocks) and flow velocity (Benn and Evans, 2010; Cuffey and Paterson, 2010).

2.4. Cosmogenic dating

Eighteen boulders were sampled for cosmogenic dating in 2013 and 2014 (indicated by sample name), and most of them were located on moraine crests (n = 14; cf.; Fig. 3). We selected the largest quartz-rich boulders (boulder heights of 30–140 cm; Heyman et al., accepted), preferentially of granitic composition (n = 16). Samples were collected from boulder top and most flat surfaces using a hammer and chisel. Location and elevation were recorded using a GPS (5 m horizontal accuracy, 10 m altitudinal accuracy). Surface dip, dip direction and topographic shielding were measured using a compass and clinometer. The detailed geomorphological context

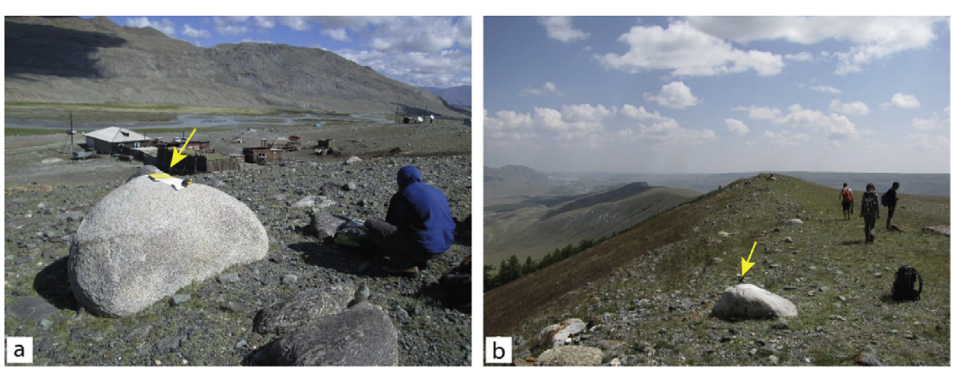

Fig. 3. Examples of granitic boulders sampled for ^{10}Be exposure dating. (a) Boulder (AL14C-01) belonging to the Beltir moraine. (b) Boulder (AL13C-30) located on a moraine ridge deposited on the top of the interfluve (cf Fig. 4). The yellow arrows indicate the boulder surfaces sampled. (For interpretation of the references to colour in this figure legend, the reader is referred to the web version of this article.)

Table 2
Details of ^{10}Be and ^{26}Al cosmogenic nuclide analyses and corresponding surface exposure ages.

Sample	Moraine complex	Location (°N/°E)	Alt. (m a.s.l.)	Thick. (cm)	Shield. Factor	[^{10}Be] (10^5 at.g^{-1})	[^{26}Al](10^5 at.g^{-1})	^{10}Be ages (ka), *Sa*	Ext. unc.	Int. unc.	^{26}Al ages (ka), *Sa*	Ext. unc.	Int. unc.	Mean and std
AL13C-30	Moraine fragment	49.95213/88.08892	2399	3	1.000	5.474 ± 0.074	39.999 ± 0.780	19.4	1.5	0.3	20.0	2.1	0.4	19.2 ± 0.4[a]
AL13C-31	on interfluve	49.95208/88.08964	2395	3	1.000	5.296 ± 0.150	38.379 ± 0.745	18.9	1.5	0.5	19.0	2.0	0.4	
AL13C-32	(up-valley)	49.95244/88.09602	2378	3	1.000	6.751 ± 0.090	36.034 ± 0.708	24.1	1.8	0.3	18.0	2.0	0.3	
AL13C-33	Moraine fragment	49.96234/88.13419	2235	1.6	0.997	4.881 ± 0.107	32.316 ± 0.949	19.4	1.5	0.4	18.2	1.9	0.5	19.4 ± 0.4[b]
AL13C-34	on interfluve (down-valley)	49.96252/88.13432	2238	2.5	1.000	7.995 ± 0.099	48.855 ± 0.810	31.4	2.4	0.4	27.2	2.9	0.4	
AL13C-26	Interfluve kame	49.94995/88.11057	2214	3	0.999	4.310 ± 0.057	29.463 ± 0.541	17.6	1.4	0.2	17.0	1.8	0.3	18.5 ± 0.8
AL13C-27	terrace	49.94995/88.10899	2227	3	0.999	4.498 ± 0.059	32.010 ± 0.536	18.2	1.4	0.2	18.0	2.0	0.3	
AL13C-28		49.94894/88.10675	2232	2.5	1.000	4.879 ± 0.108	33.941 ± 0.849	19.5	1.5	0.4	19.2	2.1	0.5	
AL13C-29		49.94883/88.10642	2232	3.5	1.000	4.629 ± 0.086	34.146 ± 0.642	18.7	1.4	0.3	19.0	2.0	0.4	
AL14C-01	Beltir Moraine	49.97573/88.17863	1982	2.3	0.999	4.318 ± 0.060	29.166 ± 0.574	20.8	1.6	0.3	20.0	2.0	0.4	19.7 ± 1.2
AL14C-02		49.97573/88.17863	1982	2.8	0.999	4.223 ± 0.063	27.187 ± 0.520	20.5	1.5	0.3	19.0	2.0	0.3	
AL14C-03		49.97489/88.17643	1988	1	1.000	3.830 ± 0.064	25.411 ± 0.563	18.3	1.5	0.3	17.1	1.8	0.4	
AL14C-04		49.97489/88.17656	1982	2.5	0.995	3.917 ± 0.062	28.829 ± 0.663	19.1	1.5	0.3	20.0	2.0	0.4	
AL13C-35	Outermost moraine	50.01659/88.35239	1952	3	1.000	3.914 ± 0.068	–	19.5	1.5	0.3	–	–		19.2 ± 1.8[c]
AL13C-36	(CUMC 1)	50.01604/88.35457	1956	3	0.998	4.341 ± 0.086	–	21.5	1.7	0.4	–	–		
AL13C-37		50.0137/88.36292	1925	2.5	1.000	6.997 ± 0.084	–	34.9	2.7	0.4	–	–		
AL13C-38		50.00481/88.3769	1876	3	0.996	3.366 ± 0.074	–	17.9	1.4	0.4	–	–		
AL13C-39		50.00429/88.3771	1876	2.5	0.990	3.316 ± 0.105	–	17.7	1.5	0.5	–	–		

The samples were measured using the ^{10}Be isotope ratio standardization 07KNSTD (Nishiizumi et al., 2007) and the ^{26}Al isotope ratio standardization KNSTD (Nishiizumi, 2004). Final ^{10}Be and ^{26}Al concentrations include measured blank corrections (correcting value based on averaged nuclide concentrations of the blanks processed during the AMS measurements of the samples): 65.204 ± 29.100 10^{-3} at.g^{-1} Be carrier and 98.209 ± 14.787 10^{-3} at.g^{-1} Al carrier for AL13C-26 to 34 and AL14C-01 to 04; 387.286 ± 39.809 10^{-3} at.g^{-1} Be carrier for AL13C-35 to 39.
All ages were calculated using the CRONUScalc program (Marrero et al., 2016), and using the CRONUS-Earth ^{10}Be and ^{26}Al production rates assessed by Borchers et al. (2016). These are minimum ages with no post-depositional erosion assumed. The adopted rock density is 2.65 g.cm^{-3}.

[a] AL13C-32 rejected for mean and standard deviation calculation, due to complex exposure history.
[b] AL13C-34 rejected for mean and standard deviation calculation, due to complex exposure history.
[c] AL13C-37 rejected for mean and standard deviation calculation, as identified as an outlier.

was recorded through notes and photographs of sample locations. Key sample information is provided in Table 2.

All samples were prepared for ^{10}Be analysis. Additionally, ^{26}Al analyses were carried out for 13 samples to investigate any potential burial-exposure history of the corresponding boulders (Lal, 1991; Nishiizumi et al., 1993; Gosse and Phillips, 2001).

Laboratory processing and measurement of the rock samples were performed at the Purdue Rare Isotope Measurement Laboratory (PRIME Lab). After sample crushing and sieving (250–500 mm), quartz was isolated following modified procedures based on Kohl and Nishiizumi (1992). Quartz was then dissolved in HF and HNO_3 and spiked with a Be carrier. Standard anion and cation exchange column procedures were used for Al and Be separation (e.g., Strelow et al., 1972; Ochs and Ivy-Ochs, 1997). Target holders (cathodes) for AMS measurements were filled with the resulting Be and Al oxides, mixed with Nb and Ag powders, respectively.

Ages were calculated using the online CRONUScalc program (Marrero et al., 2016), and using the CRONUS-Earth ^{10}Be and ^{26}Al production rates assessed by Borchers et al. (2016) (also see Phillips et al. (2016) summary paper). Ages are reported using the time- and nuclide-dependent scaling scheme LSDn (or "Sa"; Lifton et al., 2014). Topographic shielding has been accounted for in our age calculations, but not potential post-depositional surface erosion effects, as no reliable long-term erosion rates are available in the area. However, erosion rates of 1–3 mm/ka, as used by others in Central Asia (e.g. Koppes et al., 2008; Rother et al., 2014), would result in an increase of ~1–6% of the reported ages <30 ka (up to 10% for the ages >30ka).

3. Results and interpretation

3.1. Glacial geomorphology

3.1.1. Results

The Chagan Uzun Valley system is roughly oriented SW-NE and displays numerous glacial features (Figs. 1 and 4). The upper part of the system is composed of three main tributary valleys: the Chagan Valley, (draining the Akkol river), the Taldura Valley and the Kuskunnur Valley (Figs. 1 and 4), which exhibit characteristic profiles of glacial troughs. In the middle part of the system, where the three valleys join, there is a rich record of lateral moraine ridges and meltwater channels. An abrupt transition between hard bedrock, characterised by a well-developed ice-scoured landscape with numerous roches moutonnées, and soft bedrock occurs a few kilometers up-valley from the Chagan-Taldura river junction (Fig. 4). The two rivers are separated by a prominent interfluve, which also displays fragments of moraine ridges and kame terraces (Fig. 4).

Slopes of the distal, lowermost, section of the interfluve have been steepened by weathering processes and large landslides, revealing a large sedimentary section facing the Chagan River (Figs. 4 and 5).

A first set of small, well-defined frontal moraine ridges is identified close to the Chagan-Taldura drainage divide, on the Chagan valley side. The Beltir settlement is located (Fig. 4) on this feature. Downstream of this set of moraine ridges lies the most prominent geomorphological feature (>100 km^2) consisting of series of moraines expanding in the Chuja basin and exhibiting a double-lobate outline (Figs. 1 and 4). This landscape displays a multitude of narrow superimposed ridges and a few pronounced ridges with steep distal slopes (Fig. 4). The pattern and concentration of narrow ridges, combined with meltwater channels and pronounced ridges allow us to identify four different moraine complexes (Chagan Uzun Moraine Complexes, CUMC 1 (most distal) to CUMC 4, (most proximal)) in addition to the Beltir moraines. CUMC 1 and 2 exhibit a similar morphology: both form a wide and chaotic belt of multiple fragmented narrow moraine ridges of varying orientation, bordered by a pronounced well defined outer ridge with a steep distal slope. The outline of CUMC 1 describes a double lobate shape, while the CUMC 2 splays into more and smaller lobes, exhibiting a more interdigitating pattern (Fig. 4). Large lateral meltwater channels are absent in this area. CUMC 3 displays a transitional pattern from multiple chaotic narrow ridges bordered by a pronounced distal ridge, to relatively continuous and aligned narrow ridges associated with well-developed large

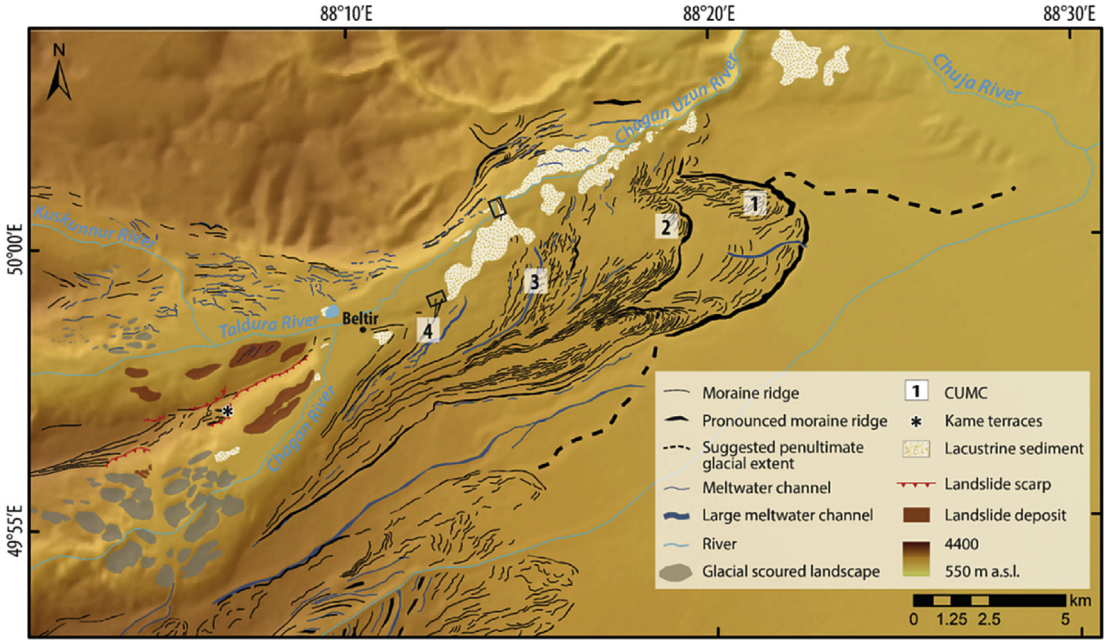

Fig. 4. Geomorphological map of the Chagan Uzun Valley, with the four Chagan Uzun Moraine Complexes (CUMC 1 to 4) and the small well-defined Beltir moraine ridges. The black boxes indicate the location of the sediment exposures a) CHU 1 and b) CHU 2. Moraine ridges and kame terraces (not visible at the scale; hence, represented by the asterisk) are also preserved on the Chagan-Taltura interfluve.

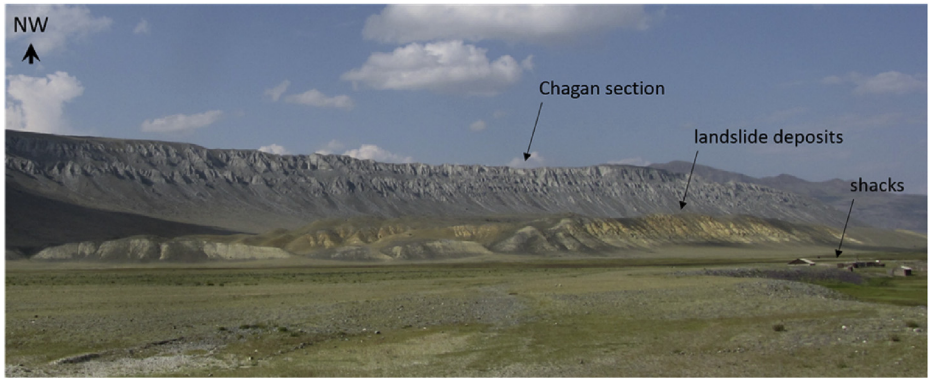

Fig. 5. View of the Chagan section (in the background) and the landslide deposits in front of it, in the Chagan Valley. The shacks are indicated for the scale.

meltwater channels in the inner part (Fig. 4). CUMC 4 clearly differs from the distal CUMCs and is more similar to the up-valley Beltir moraines, with well-defined sublinear aligned ridges curving towards the valley axis. These ridges are associated with large lateral meltwater channels.

Other noteworthy features are thick accumulations of laminated silts (>tens of meters thick) exposed along the Chagan Uzun River which cuts through the different CUMCs (Fig. 4). These deposits are also found beyond the CUMC 1. Besides, shorelines at and below c. 1970 m a.s.l. have been cut into the prominent distal sides of CUMC 1 and 2.

3.1.2. Interpretation

The ice-scoured landscape observed in the bare bedrock sections of the Chagan Uzun tributary valleys indicate the presence of a temperate glacier with a wet-based thermal regime (Sugden and John, 1976; Sugden et al., 1992; Glasser, 2002).

The three glaciers (Chagan, Taldura and Kuskunnur) that extended out of the South Chujski Range (Fig. 1) coalesced to form the Chagan Uzun glacier system at the time of CUMC 1–4 deposition. At maximum extent, this glacier system formed two coherent lobes extending into the sediment filled Chuja Basin. The widespread and chaotic occurrence of the CUMC 1 and 2 narrow moraine ridges and the well-defined steep distal margins are typical of glacial landforms resulting from the melting of stagnant ice (*hummocky moraine*; Hambrey, 1994; Evans and Rea, 2003). The numerous and multi-directional narrow ridges may correspond to the former pattern of debris within the decaying parent ice (*controlled moraine*; Benn and Evans, 1998; Evans, 2009). The presence and elevation of shorelines on the outer slopes of CUMC 1 and 2 indicate their contact with a former glacial lake in the Chuja Basin. However, the lobate shapes of the moraine complexes, their well-defined and steep distal slopes, and the absence of former subaqueous fans or gentler reworked slopes along their fringes, indicate that those units have initially been formed in a terrestrial or shallow subaqueous environment (e.g., Lønne, 1995; Powell, 2003; Ottesen and Dowdeswell, 2006). The distinct geomorphology of CUMC 4, with a succession of sub-parallel, well-defined, moraine ridges and large meltwater channels, indicates the former presence of an active glacier margin (Boulton and Eyles, 1979; Benn et al., 2003). This interpretation is valid for the Beltir moraines as well, even though they were deposited by a smaller valley glacier constrained to the lower Chagan valley. The presence in the distal section of CUMC 3 of geomorphological assemblages similar to those in glacial complexes down-valley (CUMC 1 and 2) and more ordered glacial landforms in its proximal section, might indicate two glacial events (with the latter overprinting the former), or it could reflect a transitional phase in glacier dynamics during deglaciation.

Finally, the accumulations of thinly-laminated silts observed along the Chagan Uzun River indicate the former presence of lakes. These lacustrine sediments may have been accumulated in extensive glacial lakes filling the Chuja Basin and/or within proglacial moraine-dammed lakes.

3.2. Sedimentology

The study area contains several natural exposures of sedimentary sections. The most impressive exposure, the Chagan section, is located at the distal part of the Chagan-Taldura interfluve and reveals a sediment section 200 m high and 4 km long. This section is laterally complex and can be divided into two main units: (i) a lower yellowish-brownish unit with highly oxidised and weathered sediments, interpreted as Pliocene in age based on the presence of fish that are marker fossils (Popov, 1972; Shukina, 1960) and (ii) an upper unit, composed of a Quaternary succession of glacial and glaciofluvial sediments, reflecting successive episodes of glacial advance and retreat (Shukina, 1960; Chernomorskiy et al., 1958; Popov, 1972; Rogozhin et al., 2007). However, two smaller sections directly related to the studied glacial landforms CUMC 3 and 4, CHU 1 and CHU 2 sections, are more highly relevant to an understanding of the paleo-dynamics of the Chagan Uzun Glacier system. Their sedimentological characteristics are described and interpreted below.

3.2.1. Results

3.2.1.1. Section CHU 1. This section, which has been exposed by river undercutting (50.01150°N, 88.23595°E; Fig. 4), is located in the 50 m-high proximal hillside of a moraine belt belonging to CUMC 3. The crestline of the moraine belt near the river is orientated 320° and arcs around to 225° in the south, with the hillside itself trending 145–325°. Several smaller exposures are visible throughout the hillside (Fig. 6a, b) and near the center of the arcuate moraine ridge, while a distinct exposure near the crestline furthest towards the NW is orientated almost perpendicular to the crest (190°) (Fig. 6a–d).

Sediments in the disparate exposures occur repeatedly and can be grouped into two distinct lithofacies associations (LFAs) (Fig. 6a, b). LFA 1 comprises white-yellowish rhythmically-coupled, horizontally laminated silts and clays (Flv) with individual laminae being 1–5 mm thick, separated by dark-grey, 1-2 mm-thick clay laminae. Isolated clasts of up to 1 cm are rare. Interbedded within LFA 1 are lenticular units of silty-sandy, matrix-supported, stratified diamicton (Dms) that reach 0.5 m in thickness and a maximum

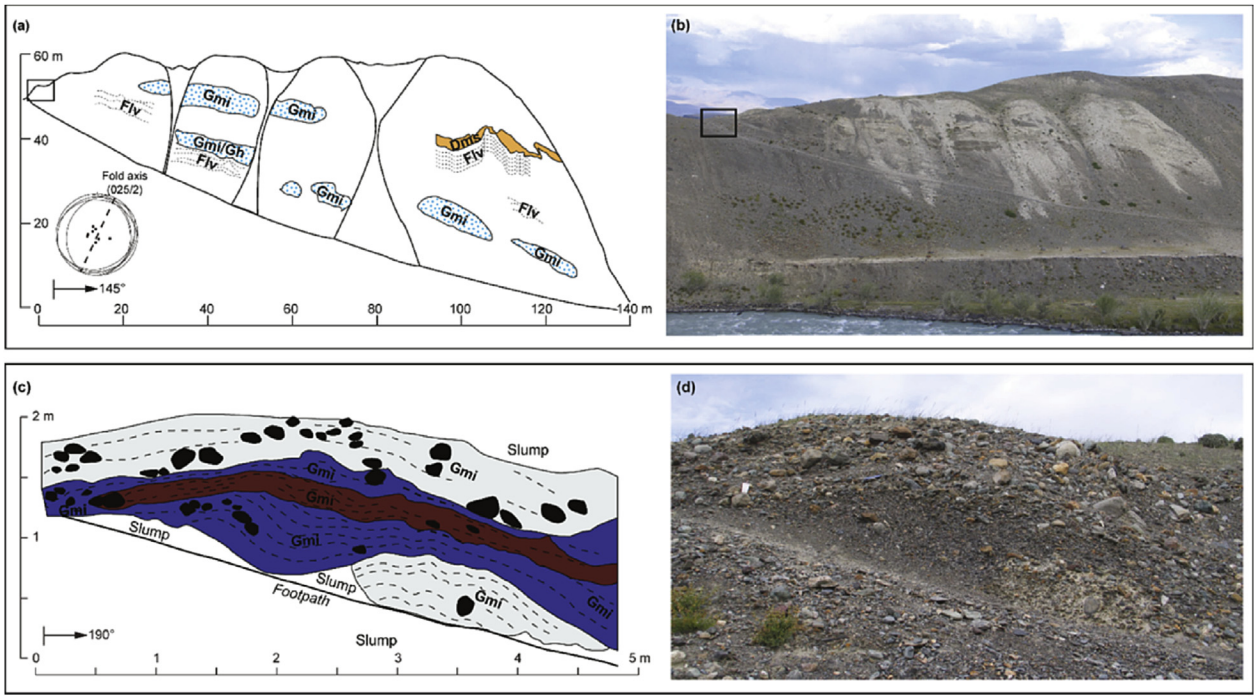

Fig. 6. (a) Scaled sketch of disparate exposures in the hillside at CHU 1, with the distinct lithofacies, and (b) photograph of the whole hillside from the opposite side of the river. Top-left frames in (a) and (b) marks the position of (c) log and (d) photograph of a clear exposure along a footpath at the top and northwestern-most point of CHU1. Here, the inflection point of an overturned fold is visible in crudely-stratified gravel units (cf LFA 2 description in 3.2.1). The inset lower-hemisphere Schmidt stereonet in (a) shows the strike and dip of measured unit contacts (solid lines), poles to planes (dots) and the calculated fold axis (dashed line).

lateral extent of 10 m. The clast content is estimated at 30–60% by area and clast sizes range from fine-gravel to boulders (0.4 m maximum a-axis length). Bullet-shapes are frequent and, visually, subangular and subrounded clasts dominate; all lithologies are local. Widespread reverse faulting has been observed throughout, with two styles of faulting, one within individual packages of laminae not thicker than ~1 m and broadly subparallel to laminae alignment; and a second dipping at >30° and traversing the thickness of entire packages of LFA 1 at the scale of several meters. Associated displacements, indicated through clear tracer horizons and folded contacts with surrounding coarser units, range from 1 to 7 cm, with the greater displacements occurring along the second type of faults. LFA 2 dominantly consists of gravels of local provenance that are horizontally-bedded (Gh) or are massive with imbricated clasts (Gmi). Individual lithofacies within LFA 2 are: (a) medium to coarse gravel clearly imbricated in a white-ish medium to coarse-sandy matrix; (b) black fine to medium massive gravel, with less-clear imbrication than in aforementioned cases; and (c) dark-grey to black medium to coarse gravel with a coarse-sandy matrix, clear imbrication and a massive appearance. Near the top of the exposure (Fig. 6c, d), these units describe a tight overturned fold-core, with gravel A-B-planes and thus imbrications following the fold. Tracing of individual LFAs across the hillslope is aided by clear colour contrasts and grain size differences. The contacts between both LFAs are sharp, with LFA 2 in places extending into the underlying LFA 1 in half-channel structures (Fig. 6a, b).

Eight undisturbed planar contacts of individual units within LFA 1 were measured across the whole hillside. During the measurements, a northern cluster emerged (n = 2) where strike and dip direction are offset by nearly 90° from the remaining (n = 6) (Fig. 6a). If all eight measurements are used, the mean fold axis strikes NE-SW (025–205°) (Fig. 6a); if the northern cluster is considered separately, it indicates a mean fold axis striking N–S (003–183°), while the mean fold axis of the remaining southerly measurements strikes 044–224°.

3.2.1.2. Section CHU 2. This exposure is part of a much-longer roadside exposure in CUMC 4 (49.986017°N, 88.213933°E; Fig. 4) and crosses most of two moraine ridges at right angles. While the outer moraine of this set of ridges, which are part of the larger complex, is not exposed, the majority of the inter-ridge sediments represent very gently-deformed (mainly buckled) laminated silts and clays (akin to LFA 1 described above), but with a notable absence of isolated clasts and diamictic units. CHU 2 is located in the distal slope of the inner moraine ridge, the crestline of which is orientated 180°, swinging around to 240° towards Beltir. The exposure contains two lithofacies (Fig. 7): The first is composed of white-yellowish rhythmically-coupled, horizontally-laminated silts and clays (Flv). The second lithofacies consists of lenses of silty-sandy, matrix-supported, stratified diamicton up to 0.25 m thick with numerous fine- to coarse-gravel pods and clasts with maximum a-axes of 0.3 m (Fig. 7b). These lenses are augen-shaped throughout, and some are folded (A in Fig. 7a). Some lenses are offset along normal and reverse faults (B in Fig. 7a; maximum displacement: 10 cm). Four measurements on normal-fault planes (1–4 in Fig. 7a) give a mean strike of 027–207°, with a mean dip of 80° to the SE. Both lithofacies units are subparallel to the distal moraine surface they underlie. Smaller exposures near the crestline and on the proximal side reveal that this subparallelism continues across the moraine, describing an anticlinal structure in phase with the land surface.

3.2.2. Interpretation

3.2.2.1. Section CHU 1. The rhythmically-laminated nature of fine-grained sediments (Flv) with isolated clasts and isolated, laterally-coherent, beds of stratified diamictons (Dms) strongly

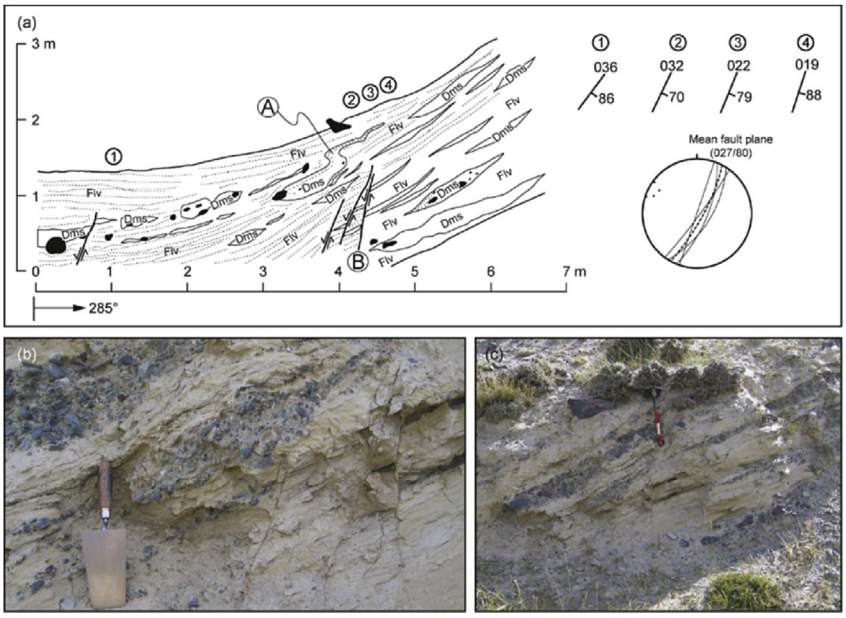

Fig. 7. (a) Log of exposure CHU 2, located in the distal slope of a moraine ridge belonging to CUMC 4, with distinct lithofacies, faults and augen-shaped lenses (also with reverse fault). (b) Close-up photograph of augen-shaped lenses just above the three prominent normal faults labelled 2–4 in (a). The trowel is ca. 28 cm long. (c) Overview photograph of section CHU 2.

indicate that LFA 1 represents a succession of glaciolacustrine sediments (e.g. Fyfe, 1990; Benn, 1996; Bennett et al., 2000). It seems likely that the majority of this succession was deposited in positions distal to the ice margin due to a relatively low occurrence of aforementioned isolated clasts, interpreted as dropstones, and a scarcity of units that indicate a higher-energy environment. However, the distinct and continuous diamicts point to a more proximal source at times. Based on their matrix component and stratification, they are interpreted as subaqueous debris flows (cf. Benn and Evans, 1993; Benn, 1996; Golledge, 2003; Lukas and Merritt, 2004). An ice margin close to this site is also consistent with the localised, sub-horizontal, non-pervasive disturbance within individual laminated packages (faults of type 1, above) (Lukas and Merritt, 2004; Phillips et al., 2007). LFA 2 structures, most notably the varying grain sizes within the coarse-sand to gravel spectrum and well-developed imbrications (Gmi), indicate a high-energy terrestrial environment that is characterised by varying water flow velocities, and is interpreted as proglacial outwash in a braided river (Collinson et al., 2006; Benn and Evans, 2010). Partial reworking of LFA 1 when LFA 2 was deposited is evident by the sharp contact and the half-channel structures which are interpreted as small scours and consistent with a relatively distal deposition of this outwash unit (cf. Marren, 2005).

The clear proglacial character of both LFAs indicates that they existed prior to being deformed into large ridges, as indicated by the overturned fold structures most clearly evident in the top part of the exposure (Fig. 6c, d). The imbrication within LFA 2 (Fig. 6c, d) is present in both limbs of the fold, demonstrating internal coherence even during folding, but also illustrating the difficulty of using imbrication as a bottom-up criterion; for this, more unequivocal sedimentary structures such as ripples in sandy units or clear gradational sequences would be necessary (Reading, 1996; Collinson et al., 2006). When the unit fragments exposed in the hillside are linked in the most intuitive manner, a large overturned fold with a fold axis broadly parallel to the crestline of the innermost moraine (orientation ~320°) can be reconstructed. However, the overall fold probably appears more distorted due to its apparent exposure rather than being exposed at right angles (cf. Twiss and Moores, 2007). Using planar unit contact measurements, tentative tracing of the change in fold axis orientation along the moraine crestline was possible, and this is broadly consistent with the overall trend of the moraine crestline from north to south (Fig. 4). Evidence for pervasive reverse faulting, potentially through the entire sedimentary package, is also consistent with high stresses imparted on the sedimentary succession, leading to brittle failure.

The sub-parallelism of the investigated fold axis with crestline orientation and the coincidence of the fold core with the top of the moraine demonstrates a clear connection between folding and moraine formation by sustained ice push (cf. Benn, 1992; Benn and Evans, 1993; Lukas, 2005, 2012; Benediktsson et al., 2008). Given that fold axes are aligned normal to the direction of stress (Twiss and Moores, 2007), the measurements indicate that the glacier in this case flowed from ~SW to ~ NE, accompanied by more local stresses acting at right angles to the former ice margin.

3.2.2.2. Section CHU 2. The lithofacies described above are highly similar to LFA 1 in section CHU 1, with the rhythmically-laminated fines (Flv) interpreted as glaciolacustrine sediments and the diamictic units (Dms) as subaqueous debris flows. However, a crucial difference at this site allows further insights into glacier dynamics to be gained, and this is the ubiquitous presence of augen shapes. These shapes provide clear indications of shearing of pre-existing sediments as they were overridden by the glacier; thus, the lithofacies at this site are interpreted as glaciotectonites (cf. Banham, 1977; Benn and Evans, 1996, 2010; Lukas, 2005; Evans et al., 2006; Lukas et al., 2012), and because mixing between Flv and Dms is very limited, this glaciotectonism is classed as non-penetrative (cf. Benn and Evans, 1996, 2010). The dip of all units is sub-parallel to distal and proximal moraine slopes and indicates the formation of this moraine by ice push, broadly consistent with glacier flow from the southwest. Finally, the mapped orientation of fault planes (297°) is also consistent with a direction of ice push at right angles, broadly from the southwest; in line with findings from

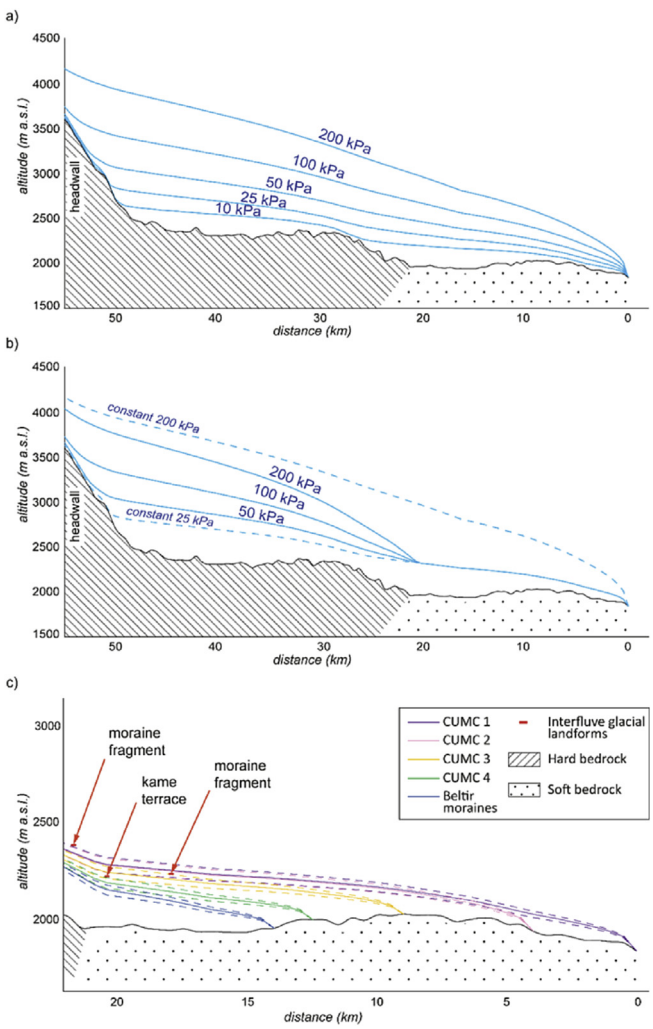

Fig. 8. Reconstructed ice surface profiles for the maximum extent of the Chagan Uzun glacier (CUMC 1) using in a) constant shear stress (10, 25, 50, 100 or 200 kPa), or in b) variable shear stresses, adapted to the bedrock type (25 kPa in the soft sediment domain; 50, 100 or 200 kPa, in the hardrock domain). Profiles with constant shear stress (25 and 200 kPa) are shown in dash lines for comparison. The figure c) displays ice surface profiles reconstructed for each identified extents, with a focus on the lower section of the profile, dominated by soft bedrock and so where low shear stress values were applied (20 kPa, represented by the full line, and 15 and 25 kPa, respectively represented by the upper and lower dash lines). The moraine fragments and kame terrace located on the interfluve and used as ^{10}Be sampling sites are also represented, to investigate the potential connections between these lateral marginal features and the frontal landforms.

Pleistocene push moraines elsewhere (e.g. Lukas, 2005, 2012). However, we cannot exclude a seismic origin of the faults.

3.3. Ice surface profile reconstructions

3.3.1. Results

The results of the ice surface profile reconstructions of the Chagan Uzun Glacier (Fig. 8) show, firstly, ice profiles calculated for its maximum extent (CUMC 1) using a range of basal shear stress (τ_B) values applied equally along the whole profile (Fig. 8a). In accordance with the input basal drag, reconstructed ice thicknesses vary significantly, with a difference of ~1000 m in the middle part of the glacier between $\tau_{B\ max} = 200$ kPa and $\tau_{B\ min} = 10$ kPa.

Secondly, ice profiles of the Chagan Uzun Glacier at its maximum extent are modelled using varying shear stresses along the profile to reflect changes in catchment geology (Fig. 8b). Indeed, the upper part of the Chagan Uzun catchment consists of glacial valley incised in hard bedrock while thick accumulations of pre-existing soft lacustrine sediments were encountered by the Chagan Uzun glacier in the lower part of the profile, at its entrance in the open Chuja basin. Therefore, a range of higher shear stresses (50–200 kPa), more appropriate for valley glaciers on hard bedrock (Cuffey and Paterson, 2010; Marshall et al., 2011), was applied to the upper domain and much lower shear stresses (≤25 kPa), consistent with values reported for unconstrained glaciers on deformable beds (e.g., Alley et al., 1987; Humphrey et al., 1993; Benn and Clapperton, 2000; Glasser and Jansson, 2005; Cuffey and Paterson, 2010) were applied to the lower domain. Diminishing the shear stress in the distal part of the profile also results in a slight lowering of the ice surface in the upper domain, even though high shear stress values are maintained in this upper area. For example, a difference of around 100 m in elevation is observed close to the headwall between the ice surface profile reconstructed using a uniform shear stress of 200 kPa and when the shear stress is decreased to 25 kPa in the lower deformable bed domain.

Finally, Fig. 8c displays ice surface profiles reconstructed for all five terminal positions identified (CUMC 1 to 4 and the Beltir moraines), with a focus on the lower part of the profile, where low values of shear stress (15–25 kPa) are applied, in agreement with the deformable nature (soft sediments) of the bed. The positions of lateral glacial landforms located on the interfluve, and used as ^{10}Be sampling sites, are also indicated. Although longer glaciers were thicker, for the same shear stress value, the difference in surface elevation between the five extents remains moderate (200 m maximum between the Beltir and CUMC 1 ice profiles).

3.3.2. Interpretation

The assumption of a constant basal shear stress along the flow line (Fig. 8a) is unrealistic considering that distinct differences in geology and geomorphology do occur. However, ice surface reconstructions using this simplistic approach still show the critical dependence of the resulting ice profiles to the basal drag applied (Fig. 8a).

A more realistic implementation of a variable basal shear stress (Fig. 8b), adapted to the encountered bedrock type, results in the reconstruction of generally thinner glaciers. According to these results, the Chagan Uzun glacier at its maximum extent still could have been either a valley glacier sourced from a cirque or nourished from an icefield/cap/dome, depending if the shear stress in the hard rock domain was rather closer to 50 kPa or 200 kPa, respectively. Unfortunately, at this stage, no more precise paleo-shear stresses can be estimated.

Finally, based on the suite of ice surface profile reconstructions performed for each of the five identified frontal positions (Fig. 8c), none of the lateral ice-marginal landforms sampled on the interfluve can be connected to the Beltir moraines. The upper and lower moraine fragments are most plausibly linked to the outer CUMC 1 or 2, and to the CUMC 1, 2 or 3, respectively. The kame terrace, at somewhat lower elevation, may instead most plausibly be linked to the CUMC 3 or CUMC 4. However, given the acknowledged uncertainties of the basal shear stress regime, it is currently not possible to establish with more precision which downvalley CUMC best connects to the interfluve glacial landforms.

3.4. Cosmogenic surface exposure results and age landform determination

Boulders sampled for surface exposure dating were collected from two moraine ridge fragments located on the top of the interfluve (n = 5), a lower kame terrace also located on the

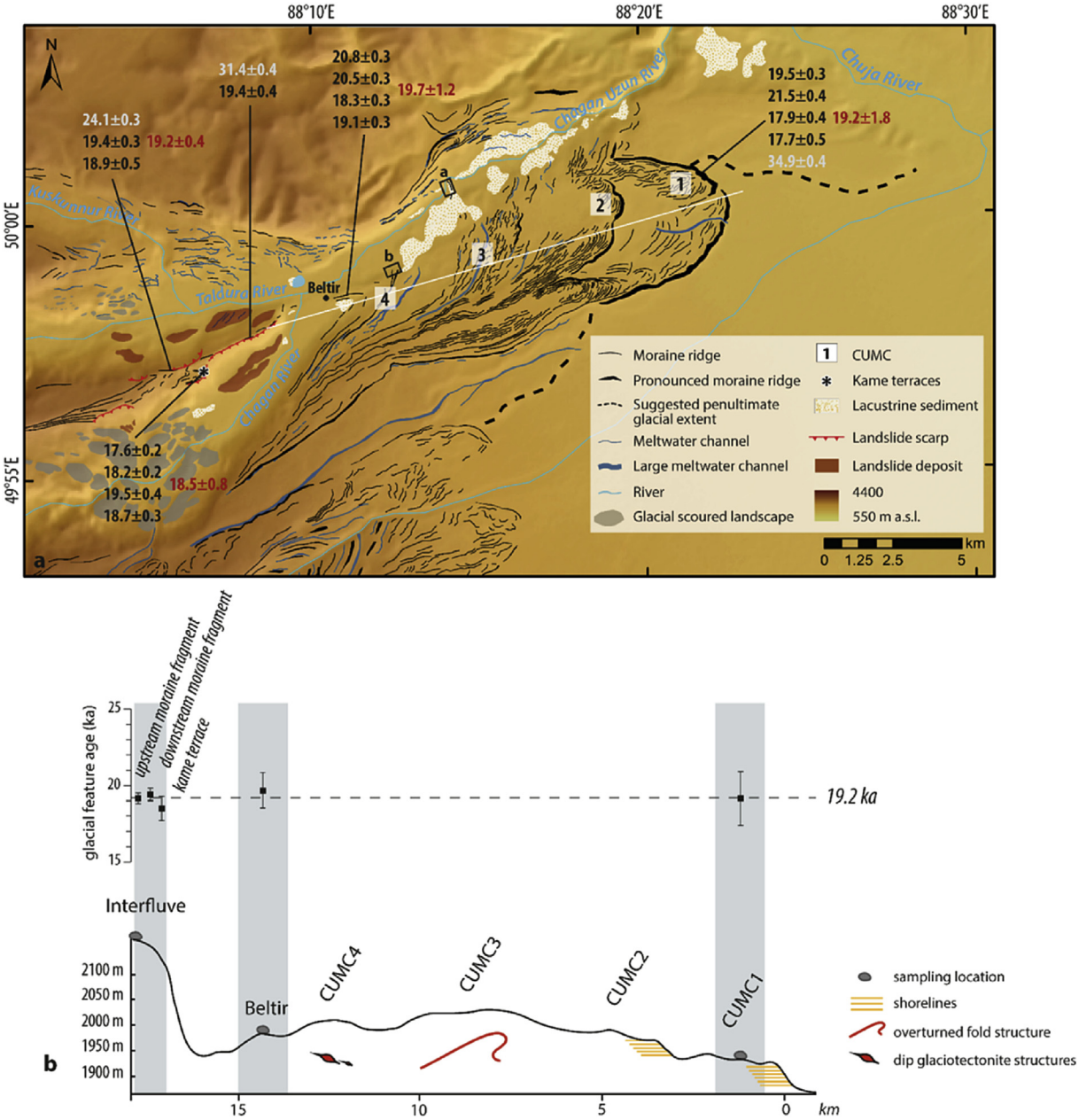

Fig. 9. Summary figure of the geomorphological, sedimentological and chronological data collected in the Chagan Uzun Valley. (a) Geomorphological map of Chagan Uzun valley with location of ^{10}Be exposure ages. Rejected ages are in grey. (b) Simplified sketch of a profile starting from the interfluve and crossing through the entire Chagan Uzun glacial deposits (white line on the map), with the indication of the main geomorphological and sedimentological features observed. The graph above indicates the global age attributed to each glacial feature sampled (link highlighted by the grey bars), equal to the mean and the standard deviation of the corresponding original ^{10}Be age data set (in red in a). All the inferred global ages are indistinguishable within their uncertainties and cluster around 19.2 ka. (For interpretation of the references to colour in this figure legend, the reader is referred to the web version of this article.)

interfluve and overlooking the Chagan River (n = 4), the Beltir moraines (n = 4), and the outermost ridge of the CUMC 1 (n = 5) (Fig. 9; Table 2). All the samples were successfully analysed.

Three samples from the interfluve moraine ridges produced ^{10}Be exposure ages between 18.9 ka and 19.4 ka and two produced older ages at 24.1 ka and 31.4 ka (Fig. 9a, Table 2). Surface exposure ages from boulders located on the interfluve kame terrace range from 17.6 ka to 19.5 ka, and from the Beltir moraine range from 18.3 ka to 20.8 ka. Finally, exposure ages from the outermost moraine range from 17.7 ka to 21.5 ka, except for one older at 34.9 ka (Fig. 9a, Table 2). Apart from the five boulders on the outermost moraine (CUMC 1), for which no ^{26}Al analyses were carried out, only two samples did not produce concordant ^{26}Al and ^{10}Be ages (AL13C-32 and 34; Table 2). These two samples, located on the interfluve moraine fragments, yielded [^{26}Al]/[^{10}Be] ratios significantly below the production rate ratio (7.1 here, based on site-specific ^{26}Al and ^{10}Be production rates), reflecting significant periods of burial (Fig. 10). These two samples also have the two oldest apparent ^{10}Be exposure ages on the interfluve, even though burial should lead to younger apparent exposure ages. These results indicate that these boulders have experienced a complex exposure history including prior exposure (inheritance) and burial periods. Those samples are therefore considered unreliable for dating the interfluve moraine fragments and are consequently rejected from further analysis and discussion. Another outlier, based on Peirce's criterion (Ross, 2003), is sample AL13C-37, located on the outermost moraine (34.9 ± 0.4

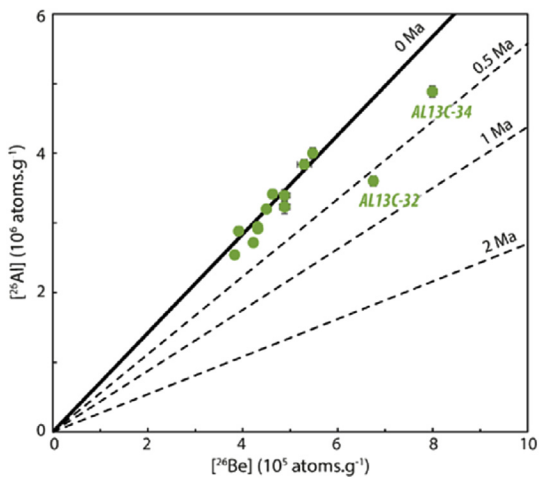

Fig. 10. [^{26}Al]-[^{10}Be] plot, assuming no erosion. The solid black line represents the [^{26}Al/^{10}Be] ratio for sample continuously exposed (7.1, based on site specific ^{26}Al and ^{10}Be production rates). The dashed lines are isochrons that correspond to burial periods of various duration. Two samples (AL13C-32 and 34) have clearly experienced considerable burial episode(s) and have therefore been rejected.

ka). Although a complex exposure history cannot be confirmed in the absence of ^{26}Al measurements, in the face of demonstrable prior exposure histories for two older samples elsewhere in the valley, we exclude this latter sample as well.

Remaining apparent exposure ages from the two interfluve moraine fragments (n = 3) are indistinguishable within their internal uncertainties (Table 2, Fig. 9a). This is not the case regarding the other features sampled, even though each chronological dataset is still relatively well clustered as their associated standard deviation does not exceed 10% of their associated mean value (Table 2, Fig. 9). One explanation for the observed scatter may be prior exposure of the boulders before deposition on the moraine, which would yield older apparent exposure ages than the true moraine age. Conversely, incomplete exposure, through exhumation of previously buried boulders due to post-depositional landform degradation processes and/or temporary post-exposure boulder surfaces coverage, can lead to apparent exposure ages that are younger than the true age of moraine formation (Putkonen and Swanson, 2003). Putkonen and Swanson (2003) and Heyman et al. (2011) suggest that incomplete exposure is more common when sampling glacial deposits, implying that the apparent older surface exposure ages should be considered as minimum ages for glacial retreat. The data reported here show that problems related to inheritance and burial (so incomplete exposure) are both present. We accordingly attribute to each sampled glacial feature a mean age and use the standard deviation as uncertainty to account for the observed scatter (Fig. 9).

With this approach, the mean ages from the different landforms are indistinguishable within uncertainty (Table 2, Fig. 9), clustering around 19.2 ka (average of landforms mean ages). This suggests that the CUMC 1, the Beltir moraines, and the interfluve moraines and kame terrace (correlated to the CUMC 1, 2 or 3 and to the CUMC 3 or 4 respectively), were deposited within a few thousand years around 19 ka (Fig. 9).

4. Discussion

4.1. Glacial landform-sediment associations in the Chagan Uzun Valley and their implications for paleoclimate reconstruction

Understanding the former dynamics of the Chagan Uzun Glacier through the origin and context of identified glacial deposits is critical for better understanding of glacier-climate interactions. Based on geomorphological and sedimentological studies, we distinguish two types of glacial landform-sediment associations in the Chagan Uzun Valley.

The first type of landform-sediment association exhibits criteria typical of alpine-style glaciations, including symmetrical cross-valley pairs of well-defined arcuate moraine ridges curving towards the valley centre, with moderate width and height (<10 m; e.g., Benn, 1992; Bennett, 1994; Benn and Lukas, 2006). These moraines are most often formed by pushing/dumping, due to oscillations of the ice margin during active retreat (e.g., Benn, 1992; Lukas, 2005; Benn and Evans, 2010). In the Chagan Uzun Valley, the Beltir moraines are the best example of this landform-sediment association (Fig. 4). Moraine ridges within CUMC 4 also exhibit a similar pattern, even though only the right-lateral arcs of the moraines pairs are preserved, presumably because the left-lateral ridges were removed by subsequent fluvial erosion. Low-amplitude folding and coexisting glaciotectonites within section CHU 2, in the CUMC 4 (Fig. 7) are evidence for low-stress ice push (deformation) and overriding episodes. These observations support the interpretation that these moraines were formed by an actively-retreating ice margin that most probably underwent stillstands and readvances (e.g., Sharp, 1984; Benn, 1992; Lukas, 2005).

The second glacial landform-sediment association, related to the outer moraine complexes, is interpreted to have been formed during surge-like events of the Chagan Uzun glacier (terminology after Lovell et al. (2012)). The identified combination of wide hummocky belts of controlled-moraine exhibiting double lobate/interdigitating terminus outlines (CUMCs 1 to 3), and hillside-scale folding accompanied by extensive faulting (observed within CUMC 3), strongly indicates a highly dynamic glacier behaviour (e.g., Evans and Rea, 2003; Schomacker and Kjær, 2007; Grant et al., 2009; Lovell, 2014). Furthermore, the presence of soft sediments, such as those encountered by the former Chagan Uzun Glacier in its foreland, has been identified as a factor favouring ice flow acceleration, especially when saturated, due to enhanced bed deformation and basal sliding processes (e.g. Anandakrishnan et al., 1998; Jiskoot et al., 2000; Lovell et al., 2012). Similar highly deformed sediments with folds several tens of meters high, and with entire moraine belts formed from the pre-existing soft sediments, thus have been observed for surging glaciers in Iceland (Benediktsson et al., 2008) and Svalbard (Rea and Evans, 2003; Lovell, 2014) and for fast flowing outlet glaciers in Patagonia (Benn and Clapperton, 2000; Lovell et al., 2012).

The ice profile reconstructions indicate that the Chagan Uzun Glacier could either have been an outlet glacier emanating from an ice field covering the South Chujski range during the glacial maximum (Blomdin et al., 2016) or been constrained to the valleys, draining then a complex catchment with at least three main tributaries, over more than 50 km. These configurations are both consistent with the suggested former surge-like behaviour of the Chagan Uzun glacier system, as surge-type glaciers have been found to frequently be associated with outlet glaciers or glaciers that show long and complex catchment areas (Jiskoot et al., 2000; Grant et al., 2009; Sevestre and Benn, 2015).

The mechanisms involved in fast ice flow/surge episodes, such as identified in the Chagan Uzun Valley, are complex and may result from a range of non-climatic internal and external factors (e.g., subglacial geology, topography, ice dynamics) (e.g., Kamb, 1987; Hamilton and Dowdeswell, 1996; Anandakrishnan et al., 1998; Jiskoot et al., 2000; Truffer and Echelmeyer, 2003; Grant et al., 2009). In these instances, the distance over which a glacier will expand cannot be straightforwardly related to climatic controls (Harrison and Post, 2003; Grant et al., 2009; Lovell et al., 2012). This is important for paleoclimate inferences as surge-related glacial

features therefore cannot be approached or quantified with traditional Equilibrium Line Altitude (ELA) reconstructions (Benn and Lehmkuhl, 2000) since this approach requires steady-state conditions with the glacier (ice mass and geometry) being in equilibrium with climate (Benn and Lehmkuhl, 2000). However, there is still a requirement for climate conditions conducive to glacier growth until, at a critical level, surging commences (e.g., Clarke et al., 1986; Dowdeswell et al., 1991; Harrison et al., 2008; Striberger et al., 2011). Based on a global compilation of surge-type glaciers, Sevestre and Benn (2015) identified an optimal "surge" climate envelope, the upper and lower limits of which are defined by linear relations between mean summer temperature (MST, in °C) and mean winter precipitation (MWP, in mm.a^{-1}). Thus surge-type glaciers do not occur above MST = 0.001*MWP+8.4 and below MST = 0.0014*MWP-0.97. Based on these boundaries, and given the local present-day MST (~12.5 °C) and MWP (~27 mm.a^{-1}) (data from Kosh-Agash weather station, Fig. 1; www.ncdc.noaa.gov), our study area is currently above the "surge" climate envelope, indicating that local past MST and MWP had to be respectively lower and higher for allowing the occurrence of the "paleo-surge". However, determining more precise past MST and MWP values based on the Sevestre and Benn (2015) climate boundaries alone is challenging. Indeed, extreme scenarios where only one climatic parameter varied, implying either a decrease of the current MST by > 4 °C or an increase of the MWP by > 4000 mm.a^{-1}, are unrealistic, especially for precipitation. Because of the wide range of possible MST-MWP combinations of intermediary values that satisfy the defined "surge" climate conditions, this prohibits, at this stage, more precise past climate inferences.

4.2. The effect of glacial lakes on cosmogenic exposure chronology

The presence and dynamics of glacial lakes potentially complicates the interpretation of apparent exposure ages from the Chagan Uzun Valley. We identify three different scenarios in which glacial lakes may impact on individual exposure ages: (a) Water may shield the sample and therefore partially or fully interrupt (depending on the water column depth) the accumulation of cosmogenic nuclides (Reuther, 2007; Dehnert and Schlüchter, 2008; Stroeven et al., 2015); (b) Toppling or tilting of boulders during high-energy drainage events (Reuther et al., 2006); and (c) Boulders have an ice-rafted origin (dropstones). Each of these scenarios would result in apparent surface exposure ages underestimating the true depositional age of the glacial feature sampled.

These scenarios are only relevant for the boulders located on features which have been covered by glacial lakes. This is not the case for the interfluve units (fragmented ridges and kame terrace), as their elevations (>2200 m a.s.l.) are above the highest shoreline reported from the Chuja Basin (2100 m a.s.l.; Carling et al., 2002). The elevation of the sampled boulders from the Beltir moraine is around 1980 m a.s.l., so below the highest shoreline found in Chuja Basin. However, the absence of shorelines or other lake-related landforms or deposits (non-reworked) in the close surroundings, at equivalent or higher elevation than the Beltir moraines, indicates that such great glacial lake episodes predate the formation of this unit. The three potential complications of glacial lakes on exposure ages have to be considered for the boulders located on the distal CUMC 1 moraine (~1875–~1955 m a.s.l) as its coverage by a glacial lake is proven by the presence of higher shorelines (up to ~1970 m a.s.l.) on the directly upstream and stratigraphically-younger CUMC 2.

4.2.1. Effect of periods of shielding by glacial lakes

A rock surface beneath water will have lower ^{10}Be production rates than one exposed subaerially. For example, ~1.5 m of water will reduce the production rate by a factor of two; and production drops to near zero for water depths ≥6 m (Reuther, 2007; Dehnert and Schlüchter, 2008). In our study, samples from boulders located on the outermost moraine (CUMC 1) produce ages ranging between 17.7 and 21.5 ka (mean age attributed to the CUMC 1: 19.2 ± 1.8 ka). Based on the difference in elevation between these boulders and the highest shorelines on the younger CUMC 2 moraine, the boulders were covered, at least once, by a water column of several tens of meters, clearly fully interrupting ^{10}Be accumulation. Although there is no doubt that the apparent CUMC 1 exposure ages underestimate the true deposition age of the unit, it is challenging to determine by how much. This will directly depend on the duration for (and depth to) which these boulders were covered by lake waters.

Herget (2005) estimated the minimum time required for complete filling of the glacial lake in the Chuja and Kuray basins to the maximum reported level (2100 m a.s.l.) to be 130 years, assuming steady climate conditions, a stationary ice dam and no loss through evaporation. This estimated time would increase considerably if losses by ice-dam leakage and evaporation were taken into account (Herget, 2005). The Kuray-Chuja glacial lake needs to have been sustained at >1960 m a.s.l. for several thousand years to have a significant impact on the cosmogenic ages, and its persistence will have entirely relied on the stability of the ice dam as no alternative spillways existed. Because ice dam stability is not only controlled by glacier oscillations, but also by a mechanical threshold above which the water accumulated cannot be supported, glacial lakes are generally short-lived features (Evans and Clague, 1994; Walder and Costa, 1996; Tweed and Russell, 1999). For example, the ice dam formed by the non-retreating Perito Moreno blocking one of Lago Argentino's lateral channels in Patagonia, has collapsed (and reformed) 17 times since the beginning of the 20th century in response to rising water level (Depetris and Pasquini, 2000; Pasquini and Depetris, 2011). Similarly, Glacial Lake Missoula, blocked by a lobe of the Cordilleran Ice sheet, drained more than 20 times over the course of a few thousand years (Hanson et al., 2012; Benito and O'Connor, 2016). Relatively short-lived glacial lakes are therefore also expected to have filled the Chuja and Kuray basins due to mechanical failure associated with rising lake levels (Tweed and Russell, 1999; Herget, 2005; Carling et al., 2010). In addition, it is likely that no large lakes developed after ~19 ka, based on the most recent large glacial lake drainage dated at ~18.7 ka by Reuther et al. (2006). Pollen diagrams from lake cores collected on the nearby Ulagan Plateau (Fig. 1) also indicate the onset of deglaciation in the area to have occurred before 16 ka (Blyakharchuk et al., 2004). No high-resolution pre-20 ka paleoclimate proxy records exist close to the study area. Ice core analysis from the Guliya ice cap, on the Qinghai-Tibetan Plateau (Thompson et al., 1997), however, indicates abrupt and oscillatory changes in temperature and pressure system over the last glacial cycle, and especially during the last glacial stage (from 15 to 33 ka). Loess sequence analysis from Kurtak, in Middle Siberia (Zander et al., 2003) indicates soil forming period interrupted by cyclic cold and dry climate conditions between 50 and 20 ka. Variations in climate indicated by both records indicate that our study area, positioned in-between these two distanced locations, was also subjected to climate oscillations. These variations were likely reflected in mass balance changes for the coalescing valley glaciers damming the Chuja River (Baker et al., 1993; Herget, 2005), as valley glaciers in this region are very sensitive to climate changes (Rupper and Roe, 2008), arguing against glacial dams maintained over long continuous periods. Furthermore, neither the terminal setting (narrow gorges), nor glacial landforms or glacier geometries (length and catchment) indicate *a-priori* that surging behaviour could also apply to the glaciers damming the Chuja river.

The apparent exposure ages underestimate the deposition time of the CUMC 1 (mean apparent age 19.2 ± 1.8 ka). However, this offset is not expected to exceed more than a few thousand years. Indeed, if the CUMC 1 was for example deposited ~30 ka, the global apparent age would require glacial lake submergence for a total period of 10 ka, which is unrealistic considering the variability of climate change over this period and mechanical factors controlling the stability of the ice dam.

4.2.2. Effects of boulder toppling during drainage events and potential dropstone origin

Reuther et al. (2006) suggested that the potential toppling of boulders during a drainage event could yield dates reflecting the drainage event itself and not the age of moraine deposition. The boulders sampled along the CUMC 1 are situated outside areas affected by strong turbulent conditions during the lake drainage, based on numerical simulation of the catastrophic drainage of the Kuray-Chuja glacial lake (Bohorquez et al., 2015) and the distribution of diluvial bedforms (Carling et al., 2002; Herget, 2005). The general morphology of the CUMC 1 is fairly well preserved, also supporting limited erosion from drainage events (Reuther, 2007). We therefore suggest that processes such as toppling and tilting of boulders have not affected the exposure history of the samples analysed in this study.

Similarly, an ice-rafted origin for the dated boulders on CUMC 1 is regarded as unlikely because all boulders, except for one sample (AL13C-38, 17.9 ± 1.4 ka), were well-embedded in the parent moraine ridge. Although AL13C-38 may be a dropstone, its age would not affect significantly the mean age determined for CUMC 1.

5. Paleoglacial history of the Chagan Uzun Valley, and paleoclimate and paleolake history

The Chagan Uzun Valley gathers a spectrum of glacial landforms reflecting a transition between two main glacial systems with very different dynamic and climatic implications. Distal moraine complexes were formed during surge-like events of outlet glaciers, or coalescing valley glaciers sustained by cold/wet conditions, while the inner glacial deposits are associated with retreat phases of temperate alpine glaciers at balance velocity (Jiskoot, 2011). Exposure ages of the outermost CUMC 1, the inner-most Beltir moraines, and glacial landforms located on the upvalley interfluve, correlated to the CUMCs 1, 2 or 3 and to CUMCs 3 or 4, indicate deposition times clustered around 19.2 ka, indistinguishable within their errors (Fig. 9). However, the actual deposition time of the outermost CUMC 1 is likely slightly underestimated due to subsequent lake water coverage. The chronological record thus indicates that the Chagan Uzun Valley experienced last glacial maximum condition during the MIS2 (14–29 ka, Lisiecki and Raymo, 2005) and a transition from glacial to deglacial conditions in a period of a few thousand years around 19 ka. This chronology agrees with IRSL ages from silt covering a moraine ridge of the CUMC 3 indicating a minimum moraine age of 22.9 ± 2.9 ka, and from sand and silt layers within till sediments related to last glacial maximum ice margins in the Kuray-Chuja basin area, ranging from 28 to 19 ka (Lehmkuhl et al., 2007, 2011).

The reconstructed glacial chronology for the Chagan Uzun Valley is also consistent with other regional and local proxies. Cold and dry conditions before 19.5 ka are indicated by major loess accumulation in Central Siberia dated to 22 ± 4 ka (Zander et al., 2003), and loess on top of fluvial terraces in the Katun River, downstream the Chuja and Kuray basins, dated to 21.3 ± 2.3 ka (Lehmkuhl et al., 2007), both using IRSL techniques. The switch from cold glacial maximum conditions to warmer interglacial conditions in this regions is best documented in the Guliya ice core, from the Qinghai-Tibetan Plateau (Thompson et al., 1997), for which the timing of the last $\delta^{18}O$ minima (associated to the coldest temperatures on record) has been estimated to 18 ± 1 ka, followed by an important rise in the $\delta^{18}O$ values. Within errors, the change in O isotopes matches the switch from glacial to deglacial conditions observed in the Chagan Uzun Valley. Finally, Reuther et al. (2006) identified and dated an outburst event suggested to be associated to the drainage of the last late Pleistocene glacial lake developed in the Kuray and Chuja basins (Reuther et al., 2006). The final lake drainage was most probably linked to a general warming of the climate as no other lakes developed subsequently. This event also should have post-dated the deposition of the CUMC 1 and 2, but pre-dated the formation of the inner Chagan Uzun deposits, based on the glacial lake shorelines only imprinted in the outer deposits. This supports the association of the drainage event with an onset of deglaciation. The recalculated cosmogenic ages, using the same production rate and scaling model as used in this study, indicate a glacial lake drainage at 18.7 ± 1.2 ka, consistent with the timing of deglaciation observed in the Chagan Uzun Valley.

6. Conclusion

The Chagan Uzun Valley exhibits the most impressive assemblage of glacial landforms and sediments in the Kuray and Chuja basins. Geomorphological and sedimentological evidence show that two different styles of glacial dynamics prevailed in this valley:

- Surge-like behaviour of glaciers formed the distal lobe-shape deposits.
- Temperate alpine glaciers at balance velocity formed the inner moraine sets during recessional phases.

The succession of moraine complexes associated with surge-like dynamic in the distal area of the Chagan Uzun Valley, and with glaciers in steady-state in the inner part, reflects a transition between glacial conditions and the retreating phase. However, because of the unsteady nature of glaciers experiencing surge-like events, the pronounced maximum extent of the former Chagan Uzun Glacier in the Chuja Basin cannot be strictly attributed to climatic control.

Cosmogenic dating of the outermost and innermost moraine complexes, and of lateral glacial landforms deposited on an interfluve and associated to intermediary phases, all indicate ages clustered around 19.2 ka. An underestimation of the age of the outermost extent of up to a few thousand years is possible due to subsequent lake water coverage. This chronology supports a Marine Isotope Stage (MIS) 2 last maximum extent of the Chagan Uzun Glacier, and an onset of deglaciation around 19 ka. This is in agreement with other local and regional paleoenvironmental regional proxies.

Acknowledgements

This work was supported by Swedish Research Council grants to Krister N. Jansson and Arjen P. Stroeven (No. 2009–4411 and 2011–4892, respectively). Additional support for fieldwork and sample processing was provided by the Swedish Society for Anthropology and Geography (SSAG) and from the Margit Alhtin and Carl Mannerfelt stipends to R. Blomdin and N. Gribenski. M.W. Caffee and N.A. Lifton acknowledge support from the U.S. National Science Foundation grant EAR-1153689. SPOT-6 images were provided through the Geoportal of Lomonosov Moscow State University.

References

Agatova, A.R., Nepop, R.K., Slyusarenko, I.Y., Myglan, V.S., Nazarov, A.N., Barinov, V.V., 2014. Glacier dynamics, palaeohydrological changes and

seismicity in southeastern Altai (Russia) and their influence on human occupation during the last 3000 years. Quat. Int. 324, 6–19.
Aizen, V.B., Aizen, E.M., Joswiak, D.R., Jujita, K., Tekeuchi, N., Nikitin, S.A., 2006. Climatic and atmospheric circulation pattern variability from ice-core isotope/geochemistry records (Altai, Tien Shan and Tibet). Ann. Glaciol. 43, 49–60.
Alexanderson, H., Murray, A.S., 2012. Luminescence signals from modern sediments in a glaciated bay, NW Svalbard. Quat. Geochronol. 10, 250–256.
Alley, R.B., Blankenship, D.D., Bentley, C.R., Rooney, S.T., 1987. Till beneath ice stream B 3. Till deformation: evidence and implications. J. Geophys. Res. 92, 8921–8929.
Anandakrishnan, S., Blankenship, D.D., Alley, R.B., Stoffa, P.L., 1998. Influence of subglacial geology on the position of a West Antarctic ice stream from seismic observations. Nature 394, 62–65.
Baker, V.R., Benito, G., Rudoy, A.N., 1993. Paleohydrology of late Pleistocene superflooding, Altay Mountains, Siberia. Science 259, 348–350.
Balco, G., 2011. Contributions and unrealized potential contributions of cosmogenic-nuclide exposure dating to glacier chronology, 1990-2010. Quat. Sci. Rev. 30, 3–27.
Banham, P.H., 1977. Glacitectonites in till stratigraphy. Boreas 6, 101–105.
Barr, I.D., Lovell, H., 2014. A review of topographic controls on moraine distribution. Geomorphology 226, 44–64.
Benediktsson, I.Ö., Möller, P., Ingólfsson, Ó., van der Meer, J.J.M., Kjær, K.H., Krüger, J., 2008. Instantaneous end moraine and sediment wedge formation during the 1890 glacier surge of Brúarjökull. Icel. Quat. Sci. Rev. 27, 209–234.
Benito, G., O'Connor, J.E., 2016. Number and size of last-glacial Missoula floods in the Columbia river valley between the Pasco Basin, Washington, and Portland, Oregon. Geol. Soc. Am. Bull. 115, 624–638.
Benn, D.I., 1992. The genesis and significance of 'hummocky moraine': evidence from the Isle of Skye, Scotland. Quat. Sci. Rev. 11, 781–799.
Benn, D.I., 1996. Subglacial and subaqueous processes near a glacier grounding line: sedimentological evidence from a former ice-dammed lake, Achnasheen, Scotland. Boreas 25, 23–36.
Benn, D.I., Evans, D.J.A., 1993. Glaciomarine deltaic deposition and ice-marginal tectonics: the 'loch Don Sand Moraine', Isle of Mull, Scotland. J. Quat. Sci. 8, 279–291.
Benn, D.I., Evans, D.J.A., 1996. The interpretation and classification of subglacially-deformed materials. Quat. Sci. Rev. 15, 23–52.
Benn, D.I., Evans, D.J.A., 1998. Glaciers and Glaciation. Arnold, London.
Benn, D.I., Clapperton, C.M., 2000. Pleistocene glacitectonic landforms and sediments around central Magellan Strait, southernmost Chile: evidence for fast outlet glaciers with cold-based margins. Quat. Sci. Rev. 19, 591–612.
Benn, D.I., Lehmkuhl, F., 2000. Mass balance and equilibrium line altitudes of glaciers in high mountain environments. Quat. Int. 65/66, 15–29.
Benn, D.I., Kirkbride, M.P., Owen, L.A., Brazier, V., 2003. Glaciated valley landsystems. In: Evans, D.J.A. (Ed.), Glacial Landsystems. Arnold, London, pp. 372–406.
Benn, D.I., Lukas, S., 2006. Younger Dryas glacial landsystems in North West Scotland: an assessment of modern analogues and palaeoclimatic implications. Quat. Sci. Rev. 25, 2390–2408.
Benn, D.I., Evans, D.J.A., 2010. Glaciers and Glaciation, second ed. Arnold, London. 802 pp.
Benn, D.I., Hulton, N.R.J., 2010. An Excel TM spread sheet program for reconstructing the surface profile of former mountain glaciers and ice caps. Comput. Geosci. 36, 605–610.
Bennett, M.R., 1994. Morphological evidence as a guide to deglaciation following the Loch Lomond Readvance: a review of research approaches and models. Scott. Geogr. Mag. 110, 24–32.
Bennett, M.R., Huddart, D., McCormick, T., 2000. The glaciolacustrine landform-sediment assemblage at Heinabergsjökull, Iceland. Geogr. Ann. 82A, 1–16.
Blomdin, R., Murray, A., Thomsen, K.J., Buylaert, J.P., Sohbati, R., Jansson, K.N., Alexanderson, H., 2012. Timing of the deglaciation in southern Patagonia: testing the applicability of K-Feldspar IRSL. Quat. Geochronol. 10, 264–272.
Blomdin, R., Heyman, J., Stroeven, A.P., Hättestrand, C., Harbor, J.M., Gribenski, N., Jansson, K.N., Petrakov, D.A., Ivanov, M.N., Alexander, O., Rudoy, A.N., Walther, M., 2016. Glacial geomorphology of the Altai and Western Sayan Mountains, Central Asia. J. Maps 12 (1), 123–136.
Blyakharchuk, T., Wright, H.E., Borodavko, P.S., Van Der Knaap, W.O., Ammann, B., 2004. Late glacial and Holocene vegetational changes on the ulagan high-mountain plateau, Altai mountains, southern Siberia. Palaeogeogr. Palaeoclimatol. Palaeoecol. 209, 259–279.
Bohorquez, P., Carling, P.A., Herget, J., 2015. Dynamic simulation of catastrophic late Pleistocene glacial-lake drainage, Altai Mountains, central Asia. Int. Geol. Rev. http://dx.doi.org/10.1080/00206814.2015.1046956.
Borchers, B., Marrero, S.M., Balco, G., Caffee, M., Goehring, B., Lifton, N., Nishiizumi, K., Phillips, F.M., Schaefer, J., Stone, J.O., 2016. Geological calibration of spallation production rates in the CRONUS-Earth project. Quat. Geochronol. 31, 188–198.
Boulton, G.S., Eyles, N., 1979. Sedimentation by valley glaciers: a model and genetic classification. In: Schluter, C. (Ed.), Moraines and Varves. Balkema, Rotterdam, pp. 11–23.
Bussemer, S., 2001. Jungquartäre Vergletscherung im Bergaltai und in angrenzenden Gebirgen- Analyse des Forschungsstandes. Mittl. Geogr. Ges. München 85, 45–64.
Butvilovsky, V.V., 1993. Last Glaciation and Holocene Palaeogeography of the Altai: Cataclysmic Model: Tomsk. Tomsk State University, 252 pp. (in Russian).
Carling, P.A., 1996. Morphology, sedimentology and palaeohydraulic significance of large gravel dunes, Altai Mountains, Siberia. Sedimentology 43, 647–664.
Carling, P.A., Kirkbride, A.D., Parnachov, S., Borodavko, P.S., Berger, G.W., 2002. Late Quaternary catastrophic flooding in the Altai Mountains of south-central Siberia: a synoptic overview and an introduction to flood deposit sedimentology. In: Martini, I.P., Baker, V.R., Garzón, G. (Eds.), Flood and Megaflood Processes and Deposits: Recent and Ancient Examples, 32. International Association of Sedimentologists, Special Publication, pp. 325–336.
Carling, P.A., Villanueva, I., Herget, J., Wright, N., Borodavko, P., Morvan, H., 2010. Unsteady 1D and 2D hydraulic models with ice dam break for Quaternary megaflood, Altai Mountains, southern Siberia. Glob. Planet. Change 70, 24–34.
Carling, P.A., Knaapen, M., Borodvako, P., 2011. Palaeoshorelines of Glacial Lake Kuray-Chuja, South-central Siberia: Form, Sediments and Process, 354. Geological Society, London, pp. 111–128. Special Publications.
Cerling, T.E., Craig, H., 1994. Geomorphology and in-situ cosmogenic isotopes. Annu. Rev. Earth Planet. Sci. 22, 273–317.
Chernomorskiy, M.A., Musienko, Z.V., Rakovets, O.A., Trifonov, N.P., 1958. USSR Geological Map, 1:200 000, Gorny Altai Series, M-45-XXIII, XXIX. Ministry of Geology and Preservation of Natural Resources.
Clarke, G.K.C., Schmok, J.P., Ommanney, C.S.L., Collins, S.G., 1986. Characteristics of surge-type glaciers. J. Geophys. Res. 91 (B7), 7165–7180.
Cockburn, H., Summerfield, M.A., 2004. Geomorphological applications of cosmogenic isotope analysis. Prog. Phys. Geogr. 28, 1–42.
Collinson, J.D., Mountney, N.P., Thompson, D.B., 2006. Sedimentary Structures, third ed. Terra Publishing, Harpenden. 292 pp.
Cuffey, K.M., Paterson, W.S.B., 2010. The Physics of Glaciers, fourth ed. Butterworth-Heinemann, Oxford, UK. 693 pp.
Dehnert, A., Schlüchter, C., 2008. Sediment burial dating using terrestrial cosmogenic nuclides. Eiszeitalter und Gegenwart. Quat. Sci. J. 57, 210–225.
Delvaux, D., Theunissen, K., Van der Meer, R., Berzin, N., 1995. Dynamics and paleostress of the Cenozoic Kurai-Chuya depression of Gorny Altai (South Siberia): tectonic and climatic control. Russ. Geol. Geophys. 36, 26–45.
Depetris, P.J., Pasquini, A.I., 2000. The hydrological signal of the Moreno glacier damming of lake Argentino (Southern Andean Patagonia): the ENSO connection. Glob. Planet. Change 26, 367–374.
Dmitrieva, V.K., Volochkovich, K.L., Savosina, A.K., Shmidt, G.A., 1959. USSR Geological Map, 1:200 000, Gorny Altai Series, M-45-XXII, XXVIII. Ministry of Geology and Preservation of Natural Resources.
Dowdeswell, J.A., Hamilton, G.S., Hagen, J.O., 1991. The duration of the active phase on surge-type glaciers: contrasts between Svalbard and other regions. J. Glaciol. 37, 388–400.
Duller, G.A.T., 2006. Single grain optical dating of glacigenic deposits. Quat. Geochronol. 1, 296–304.
Evans, D.J.A., 2009. Controlled moraines: origins, characteristics and palaeoglaciological implications. Quat. Sci. Rev. 28, 183–208.
Evans, S.G., Clague, J.J., 1994. Recent climatic change and catastrophic geomorphic processes in mountain environments. Geomorphology 10, 107–128.
Evans, D.J.A., Rea, B.R., 2003. Surging glacier landsystem. In: Evans, D.J.A. (Ed.), Glacial Landsystems. Arnold, London, pp. 259–288.
Evans, D.J.A., Benn, D.I., 2004. A Practical Guide to the Study of Glacial Sediments. Arnold, London, p. 266.
Evans, D.J.A., Phillips, E.R., Hiemstra, J.F., Auton, C.A., 2006. Subglacial till: formation, sedimentary characteristics and classification. Earth Sci. Rev. 78, 115–176.
Fabel, D., Harbor, J., 1999. The use of in-situ produced cosmogenic radionuclides in glaciology and glacial geomorphology. Ann. Glaciol. 28, 103–110.
Forman, S.L., 1988. The solar resetting of thermoluminescence of sediments in a glacier-dominated fiord environment in Spitsbergen: geochronology implications. Arct. Alp. Res. 20, 243–253.
Fyfe, G., 1990. The effect of water depth on ice-proximal glaciolacustrine sedimentation: Salpausselkä I, southern Finland. Boreas 19, 147–164.
Gemmell, A.M.D., 1988. Thermoluminescence dating of glacially transported sediments: some considerations. Quat. Sci. Rev. 7, 277–285.
Glasser, N.F., 2002. The large Roches moutonnées of upper Deeside. Scott. Geogr. J. 118 (2), 129–138.
Glasser, N.F., Jansson, K.N., 2005. Fast-flowing outlet glaciers of the last glacial maximum Patagonian icefield. Quat. Res. 63, 206–211.
Glasser, N.F., Jansson, K.N., Harrison, S., Rivera, A., 2005. Geomorphological evidence for variations of the North Patagonian icefield during the Holocene. Geomorphology 71, 263–277.
Golledge, N.R., 2003. A former ice-dammed lake in Glen Luibeg, Cairngorm Mountains, Scotland. Quat. Newsl. 101, 13–24.
Gosse, J.C., Phillips, F.M., 2001. Terrestrial in situ cosmogenic nuclides: theory and application. Quat. Sci. Rev. 20, 1475–1560.
Grant, K.L., Stokes, C.R., Evans, I.S., 2009. Identification and characteristics of surge-type glaciers on Novaya Zemlya, Russian Arctic. J. Glaciol. 55, 960–972.
Hambrey, M., 1994. Glacial Environments. UCL Press, London, 304 pp.
Hamilton, G.S., Dowdeswell, J.A., 1996. Controls on glacier surging in Svalbard. J. Glaciol. 42, 157–168.
Hanson, M.A., Lian, O.B., Clague, J.J., 2012. The sequence and timing of large late Pleistocene floods from glacial Lake Missoula. Quat. Sci. Rev. 31, 67–81.
Harrison, W.D., Post, A.S., 2003. How much do we really know about glacier surging? Ann. Glaciol. 36, 1–6.
Harrison, W.D., Eisen, O., Fahnestock, M.A., Moran, M.T., Motyka, R.J., Nolan, M., Raymond, C.F., 2008. Another surge of variegated glacier, Alaska, USA, 2004/04. J. Glaciol. 54 (184), 192–194.

Herget, J., 2005. Reconstruction of ice-dammed lake outburst floods in the Altai mountains, Siberia. In: Geological Society of America, Special Paper 386. Geological Society of America, Boulder, Colorado, 118 pp.
Heyman, J., Stroeven, A.P., Harbor, J.M., Caffee, M.W., 2011. Too young or too old: evaluating cosmogenic exposure dating based on an analysis of compiled boulder exposure ages. Earth Planet. Sci. Lett. 302, 71–80.
Heyman, J., Applegate, P.J., Blomdin, R., Gribenski, N., Harbor, J.M., Stroeven, A.P., accepted. Boulder height-exposure age relationships from a global glacial ^{10}Be compilation. Quat. Geochronol..
Holcombe, R., 2010. GeOrient v9.x. http://www.holcombe.net.au/software/rodh_software_georient.htm. Last accessed 15.09.2015.
Humphrey, N., Kamb, B., Fahnestock, M., Engelhardt, H., 1993. Characteristics of the bed of the lower Columbia Glacier, Alaska. J. Geophys. Res. 98, 837–846.
Jiskoot, H., 2011. Dynamics of glaciers. In: Singh, V.P., Singh, P., Haritashya, U.K. (Eds.), Encyclopedia of Snow, Ice and Glaciers. Springer, Dordrecht, The Netherlands, pp. 245–256.
Jiskoot, H., Murray, T., Boyle, P., 2000. Controls on the distribution of surge-type glaciers in Svalbard. J. Glaciol. 46, 412–422.
Jomelli, V., Favier, V., Rabatel, A., Brunstein, D., Hoffmann, G., Francou, B., 2009. Fluctuations of glaciers in the tropical Andes over the last millennium and palaeoclimatic implications: a review. Palaeogeogr. Palaeoclimatol. Palaeoecol. 281, 269–282.
Kamb, B., 1987. Glacier surge mechanism based on linked cavity configuration of the basal water conduit system. J. Geophys. Res. 92, 9083–9100.
Kirkbride, M.P., Brazier, V., 1998. A critical evaluation of the use of glacier chronologies in climatic reconstruction, with reference to New Zealand. Quat. Res. Assoc. 6, 55–64.
Kirkbride, M.P., Winkler, S., 2012. Correlation of Late Quaternary moraines: impact of climate variability, glacier response, and chronological resolution. Quat. Sci. Rev. 46, 1–29.
Kohl, C., Nishiizumi, K., 1992. Chemical isolation of quartz for measurement of in-situ produced cosmogenic nuclides. Geochim. Cosmochim. Acta 56, 3583–3587.
Koppes, M., Gillespie, A.R., Burke, R.M., Thompson, S.C., Stone, J., 2008. Late quaternary glaciation in the Kyrgyz Tien Shan. Quat. Sci. Rev. 27, 846–866.
Lal, D., 1991. Cosmic ray labeling of erosion surfaces: in situ nuclide production rates and erosion rates. Earthand Planet. Sci. Lett. 104, 424–439.
Lehmkuhl, F., Frechen, M., Zander, A., 2007. Luminescence chronology of fluvial and aeolian deposits in the Russian Altai (southern Siberia). Quat. Geochronol. 2, 195–201.
Lehmkuhl, F., Klinge, M., Stauch, G., 2011. The extent and timing of Late Pleistocene glaciations in the Altai and neighbouring mountain systems. In: Ehlers, J., Gibbard, P.L., Hughes, P.D. (Eds.), Developments in Quaternary Science - Extent and Chronology - a Closer Look, 15, pp. 967–979.
Lifton, N., Sato, T., Dunai, T.J., 2014. Scaling in situ cosmogenic nuclide production rates using analytical approximations to atmospheric cosmic-ray fluxes. Earth Planet. Sci. Lett. 386, 149–160.
Lisiecki, L.E., Raymo, M.E., 2005. A Pliocene-Pleistocene stack of 57 globally distributed benthic ^{18}O records. Paleoceanography 20, 1–17.
Lønne, I., 1995. Sedimentary facies and depositional architecture of ice-contact glaciomarine systems. Sediment. Geol. 98, 13–43.
Lovell, H., 2014. On the Ice-sediment-landform Associations of Surging Glaciers on Svalbard. Unpublished PhD thesis. Queen Mary University of London, School of Geography, 295 pp.
Lovell, H., Stokes, C.R., Bentley, M.J., Benn, D.I., 2012. Evidence for rapid ice flow and proglacial lake evolution around the central Strait of Magellan region, southernmost Patagonia. J. Quat. Sci. 27 (6), 625–638.
Lukas, S., 2005. A test of the englacial thrusting hypothesis of 'hummocky' moraine formation - case studies from the north-west Highlands, Scotland. Boreas 34, 287–307.
Lukas, S., 2012. Processes of annual moraine formation at a temperate alpine valley glacier: insights into glacier dynamics and climatic controls. Boreas 41, 463–480.
Lukas, S., Merritt, J.W., 2004. Evidence for a former ice-dammed lake in Coire Mhicsith. In: Lukas, S., Merritt, J.W., Mitchell, W.A. (Eds.), The Quaternary of the Central Grampian Highlands: Field Guide. Quaternary Research Association, London, pp. 149–158.
Lukas, S., Spencer, J.Q.G., Robinson, R.A.J., Benn, D.I., 2007. Problems associated with luminescence dating of Late Quaternary glacial sediments in the NW Scottish Highlands. Quat. Geochronol. 2, 243–248.
Lukas, S., Graf, A., Coray, S., Schlüchter, C., 2012. Genesis, stability and preservation potential of large lateral moraines of Alpine valley glaciers - towards a unifying theory based on Findelengletscher, Switzerland. Quat. Sci. Rev. 38, 27–48.
Margold, M., Jansson, K.N., Stroeven, A.P., Jansen, J.D., 2011. Glacial Lake vitim, a 3000-km3 outburst flood from Siberia to the arctic ocean. Quat. Res. 76, 393–396.
Markov, K.K. (Ed.), 1978. Section the Latest Deposits of the Altai. Izdatel'stvo Moscowskogo Universiteta, Moscow, 208 pp. (in Russian).
Marren, P.M., 2005. Magnitude and frequency in proglacial rivers: a geomorphological and sedimentological perspective. Earth Sci. Rev. 70, 203–251.
Marrero, S.M., Phillips, F.M., Borchers, B., Lifton, N., Aumer, R., Balco, G., 2016. Cosmogenic nuclide systematics and the CRONUScalc program. Quat. Geochronol. 31, 160–187.
Marshall, S.J., White, E.C., Denuth, M.N., Bolch, T., Wheate, R., Menounos, B., Beedle, M.J., Shea, J.M., 2011. Glacier water resources on the eastern slopes of the Canadian Rocky Mountains. Can. Water Resour. J./Revue Can. des ressources hydriques 36, 109–134.
Nishiizumi, K., 2004. Preparation of 26Al AMS standards. Nucl. Instrum. Methods Phys. Res. B 223, 388–392.
Nishiizumi, K., Kohl, C.P., Arnold, J.R., 1993. Role of in-situ cosmogenic nuclides ^{10}Be and ^{26}Al in the study of diverse geomorphic processes. Earth Surf. Process. Landforms 18, 407–425.
Nishiizumi, K., Imamura, M., Caffee, M.W., Southon, J.R., Finkel, R.C., McAninch, J., 2007. Absolute calibration of ^{10}Be AMS standards. Nucl. Instrum. Methods Phys. Res. B 258, 403–413.
Novikov, I.S., 1988. Geology-geomorphological Research in the Mountain Altai. Bibliography for 1836-1986. Novosibirsk. Institution of Geology and Geophysics, 68 pp. (in Russian).
Obruchev, V.A., 1914. Altai essays (Essay first). Notes on tracks of ancient glaciation in the Russian Altai. Geography 4, 50–93 (In Russian).
Ochs, M., Ivy-Ochs, S., 1997. The chemical behavior of Be, Al, Fe, Ca and Mg during AMS target preparation from terrestrial silicates modeled with chemical speciation calculations. Nucl. Instrum. Methods Phys. Res. B 123, 235–240.
Okishev, P.A., 1982. Dynamic of Glaciations in Altai during Late-pleistocene and Holocene. Tomsk, Iadatel'stvo Tomskogo Universiteta, 209 pp. (in Russian).
Ottesen, D., Dowdeswell, J.A., 2006. Assemblages of submarine landforms produced by tidewater glaciers in Svalbard. J. Geophys. Res. 111, 1–16.
Pasquini, A.I., Depetris, P.J., 2011. Southern Patagonia's Perito Moreno glacier, lake Argentino, and Santa Cruz river hydrological system: an overview. J. Hydrol. 405, 48–56.
Phillips, E.R., Merritt, J.W., Auton, C.A., Golledge, N.R., 2007. Microstructures in subglacial and proglacial sediments: understanding fault, folds and fabric and the influence of water on the style of deformation. Quat. Sci. Rev. 26, 1499–1528.
Phillips, F.M., Argento, D.C., Balco, G., Caffee, M.W., Clem, J., Dunai, T., Finkel, R., Goehring, B., Gosse, J.C., Hudson, A., Jull, T.A., Kelly, M., Kurz, M., Lal, D., Lifton, N., Marrero, S.M., Nishiizumi, K., Reedy, R., Schaefer, J., Stone, J.O., Swanson, T., Zreda, M.G., 2016. The cronus-earth project: a synthesis. Quat. Geochronol. 31, 119–154.
Popov, V.E., 1962. On closed systems of marginal glacier formations in valleys of South-Western corner of Chyia steppe in the Mountain Altai. Glaciology of Altai. Tomsk 1, 188–221 (in Russian).
Popov, V.E., 1972. The possibility of using geomorphological criteria to determine the age of the Quaternary deposits in Chagan-Uzun reference outcrop Altai. Altai Glaciology 7. Tomsk 104–114 (in Russian).
Powell, R.D., 2003. Subaquatic landsystems:fjords. In: Evans, D.J.A. (Ed.), Glacial Landsystmes. Arnold, London, pp. 313–347.
Putkonen, J., Swanson, T., 2003. Accuracy of cosmogenic ages for moraines. Quat. Res. 59, 255–261.
Rea, B.R., Evans, D.J.A., 2003. Plateau icefield landsystems. In: Evans, D.J.A. (Ed.), Glacial Landsystems. Arnold, pp. 407–431.
Reading, H.G. (Ed.), 1996. Sedimentary Environments: Processes, Facies and Stratigraphy, third ed. Blackwell, Oxford.
Reuther, A.U., 2007 (PhD thesis). Surface Exposure Dating of Glacial Deposits Form the Last Glacial Cycle. Evidence from the Eastern Alps, the Bavarian Forest, the Southern Carpathians and the Altai Mountains, 21. Relief Boden Paläoklima, p. 246.
Reuther, A.U., Herget, J., Ivy-Ochs, S., Borodavko, P., Kubik, P.W., Heine, K., 2006. Constraining the timing of the most recent cataclysmic flood event from ice-dammed lakes in the Russian Altai Mountains, Siberia, using cosmogenic in situ ^{10}Be. Geology 34, 913–916.
Rogozhin, E.A., Ovsyuchenko, A.N., Marakhanov, A.V., Ushanova, E.A., 2007. Tectonic setting and geological manifestations of the 2003 Altai Earthquake. Geotectonics 41, 87–104.
Ross, S.M., 2003. Peirce's criterion for the elimination of suspect experimental data. J. Eng. Technol. 20, 38–41.
Rother, H., Lehmkuhl, F., Fink, D., Nottebaum, V., 2014. Surface exposure dating reveals MIS-3 glacial maximum in the Khangai Mountains of Mongolia. Quat. Res. 82, 297–308.
Rudoy, A.N., 1981. To the history of pre-glacial lakes of Chuya Basin, Altai mountains. Data of glaciological research. Acad. Sci. USSR 41, 213–218 (in Russian).
Rudoy, A.N., 1998. Mountain ice-dammed lakes of Southern Siberia and their influence on the development and regime of the intracontinental runoff systems of North Asia in the late Pleistocene. In: Benito, G., Baker, V.R., Gregory, K.J. (Eds.), Palaeohydrology and Environmental Change. Wiley, Chichester, pp. 215–234.
Rudoy, A.N., 2002. Glacier-dammed lakes and geological work of glacial superfloods in the late Pleistocene, southern Siberia, Altai mountains. Quat. Int. 87/1, 119–140.
Rudoy, A.N., Baker, V.R., 1993. Sedimentary effects of cataclysmic late Pleistocene glacial outburst flooding, Altay Mountains, Siberia. Sediment. Geol. 85, 53–62.
Rupper, S.B., Roe, G.H., 2008. Glacier changes and regional climate - a mass and energy balance approach. J. Clim. 21, 5384–5401.
Rusanov, G.G., 2008. Maximal level of Chuya glacier-dammed lake in the Mountain Altai. Geomorphology 1, 65–71 (In Russian).
Rusanov, G.G., 2010. The Holocene climate changes in Chuya depression (Gorny Altai) on the basis of ostracod fauna analysis (Izmenenija klimata Chujskoj kotloviny Gornogo Altaja v golocene po faune ostracod). Prog. Mod. Nat. Sci. [Uspehi sovremennogo estestvoznanija] 10, 20–25 (in Russian).
Sapozhnikov, V.V., 1911. Trails through Russian Altai. Tomsk, 169 pp.

Schaefer, J.M., Denton, G.H., Barrell, D.J.A., Ivy-Ochs, S., Kubik, P.W., Andersen, B.G., Phillips, F.M., Lowell, T.V., Schlüchter, C., 2006. Near-synchronous interhemispheric termination of the last glacial maximum in mid-latitudes. Science 312, 1510–1513.
Schomacker, A., Kjær, K.H., 2007. Origin and de-icing of multiple generations of icecored moraines at Brúarjökull. Icel. Boreas 36, 411–425.
Sevestre, H., Benn, D.I., 2015. Climatic and geometric controls on the global distribution of surge-type glaciers: implications for a unifying model of surging. J. Glaciol. 61, 646–662.
Shahgedanova, M., Nosenko, G., Khromova, T., Muraveyev, A., 2010. Glacier shrinkage and climatic change in the Russian Altai from the mid-20th century: an assessment using remote sensing and PRECIS regional climate model. J. Phys. Res. 115, 1–12.
Sharp, M.J., 1984. Annual moraine ridges at Skalafellsjökull, south-east Iceland. J. Glaciol. 30, 82–93.
Shukina, E.N., 1960. Patterns of distribution and stratigraphy of Quaternary sediments in the territory of the Altai. Tr. GIN AN SSSR 26, 127–164 (in Russian).
Sheinkman, V.S., 2011. Glaciation in the high mountains of Siberia. In: Ehlers, J., Gibbard, P.L., Hughes, P.D. (Eds.), Developments in Quaternary Science, 15, pp. 883–907.
Solomina, O., Haeberli, W., Kull, C., Wiles, G., 2008. Historical and Holocene glacier–climate variations: general concepts and overview. Glob. Planet. Change 60, 1–9.
Stone, J.O., 2000. Air pressure and cosmogenic isotope production. J. Geophys. Res. 105, 23 753–23 759.
Strelow, F., Weinert, C., Eloff, C., 1972. Distribution coefficients and anion exchange behavior of elements in oxalic acid-hydrochloric acid mixtures. Anal. Chem. 44, 2352–2356.
Striberger, J., Björck, S., Benediktsson, I.Ö., Snowball, I., Uvo, C., Ingólfsson, Ó., Kjaer, K.H., 2011. Climatic control of the surge periodicity of an Icelandic outlet glacier. J. Quat. Sci. 26, 561–565.
Stroeven, A.P., Hättestrand, C., Heyman, J., Kleman, J., Morén, B.M., 2013. Glacial geomorphology of the Tian Shan. J. Maps 9, 505–512.
Stroeven, A.P., Heyman, J., Fabel, D., Björck, S., Caffee, M.W., Fredin, O., Harbor, J.M., 2015. A new Scandinavian reference ^{10}Be production rate. Quat. Geochronol. 29, 104–115.
Sugden, D.E., John, B., 1976. Glaciers and Landscape. Edward Arnold publishers, London.
Sugden, D.E., Glasser, N.F., Clapperton, C.M., 1992. Evolution of large roches moutonnees. Geogr. Ann. 74A, 253–264.
Svitoch, A.A., 1978. On age of glacial and fluvioglacial sediments in Chagan-Uzun catchment (Mountain Altai). Herald of MSU, Series 5. Geography 4, 114–116 (in Russian).
Svitoch, A.A., Parunin, O.G., 1976. On age of the terminal moraine in Chagan-Uzun valley (Mountain Altai). Glaciology of Altai. Tomsk 10, 102–103 (in Russian).
Thompson, L.G., Yao, T., Davis, M.E., Henderson, K.A., Thompson, E.M., Lin, P.N., Beer, J., Synal, H.A., Cole-Dai, J., Bolzan, J.F., 1997. Tropical climate instability: the last glacial cycle from a QinghaieTibetan ice core. Science 276, 1821–1825.
Truffer, M., Echelmeyer, K.A., 2003. Of isbrae and ice streams. Ann. Glaciol. 36, 66–72.
Tweed, F.S., Russell, A.J., 1999. Controls on the formation and sudden drainage of glacier-impounded lakes: implications for jökulhlaup characteristics. Prog. Phys. Geogr. 23, 79–110.
Twiss, R.J., Moores, E.M., 2007. Structural Geology, second ed. Freeman, New York. 736 pp.
Walder, J.S., Costa, J.E., 1996. Outburst floods from glacier-dammed lakes: the effect of mode of lake drainage on flood magnitude. Earth Surf. Process. Landforms 21, 701–723.
Zander, A., Frechen, M., Zykina, V., Boenigk, W., 2003. Luminescence chronology of the upper Pleistocene loess record at Kurtak in middle Siberia. Quat. Sci. Rev. 22, 999–1010.